

# Dynamic Multiple-Parameter Joint Time-Vertex Fractional Fourier Transform and its Intelligent Filtering Methods

Manjun Cui, Ziqi Yan, Yangfan He, and Zhichao Zhang, *Member, IEEE*

**Abstract**—Dynamic graph signal processing provides a principled framework for analyzing time-varying data defined on irregular graph domains. However, existing joint time-vertex transforms such as the joint time-vertex fractional Fourier transform assign only one fractional order to the spatial domain and another one to the temporal domain, thereby restricting their capacity to model the complex and continuously varying dynamics of graph signals. To address this limitation, we propose a novel dynamic multiple-parameter joint time-vertex fractional Fourier transform (DMPJFRFT) framework, which introduces time-varying fractional parameters to achieve adaptive spectral modeling of dynamic graph structures. By assigning distinct fractional orders to each time step, the proposed transform enables dynamic and flexible representation of spatio-temporal signal evolution in the joint time-vertex spectral domain. Theoretical properties of the DMPJFRFT are systematically analyzed, and two filtering approaches: a gradient descent-based method and a neural network-based method, are developed for dynamic signal restoration. Experimental results on dynamic graph and video datasets demonstrate that the proposed framework effectively captures temporal topology variations and achieves superior performance in denoising and deblurring tasks compared with some state-of-the-art graph-based transforms and neural networks.

**Index Terms**—Dynamic graph signal, filtering, graph neural networks, multiple-parameter.

## I. INTRODUCTION

As data becomes increasingly structured in complex systems such as social networks, transportation systems, sensor networks, and bioinformatics networks, traditional signal processing (SP) methods defined in Euclidean space are no longer able to effectively characterize the irregular relationships inherent in such data. Graph signal processing (GSP) has emerged as a systematic theoretical framework for defining, analyzing, and

This work was supported in part by the Open Foundation of Hubei Key Laboratory of Applied Mathematics (Hubei University) under Grant HBAM202404; in part by the Foundation of Key Laboratory of System Control and Information Processing, Ministry of Education under Grant Scip20240121; and in part by the Startup Foundation for Introducing Talent of Nanjing Institute of Technology under Grant YKJ202214. (*Corresponding author: Zhichao Zhang*.)

Manjun Cui and Ziqi Yan are with the School of Mathematics and Statistics, Nanjing University of Information Science and Technology, Nanjing 210044, China (e-mail: cmj1109@163.com; yanziqi54@gmail.com).

Yangfan He is with the School of Communication and Artificial Intelligence, School of Integrated Circuits, Nanjing Institute of Technology, Nanjing 211167, China (e-mail: Yangfan.He@njit.edu.cn).

Zhichao Zhang is with the School of Mathematics and Statistics, Nanjing University of Information Science and Technology, Nanjing 210044, China, with the Hubei Key Laboratory of Applied Mathematics, Hubei University, Wuhan 430062, China, and also with the Key Laboratory of System Control and Information Processing, Ministry of Education, Shanghai Jiao Tong University, Shanghai 200240, China (e-mail: zzc910731@163.com).

processing signals on graphs [1]–[3]. In recent years, GSP has demonstrated broad application potential in fields such as social relationship analysis, recommender systems, traffic flow prediction, and brain functional connectivity modeling [4]–[9].

Within the framework of GSP, spectral analysis plays a crucial role in characterizing the structural and functional properties of graph signals. Among the commonly used spectral methods, the graph Fourier transform (GFT) [10]–[15] and the graph fractional Fourier transform (GFRFT) [16]–[21] enable the extraction of spatial-frequency features from graph signals. However, these methods are limited in that they cannot directly capture temporal-frequency characteristics, which are essential for modeling signals that evolve over time. To jointly extract spatio-temporal frequency characteristics, researchers proposed the joint time-vertex Fourier transform (JFT) [22], [23]. Later, the fractional-order concept is introduced to extend JFT into the joint time-vertex fractional Fourier transform (JFRFT) [20], [21], [24], which provides a parameterized spectral transformation. Despite these improvements, existing JFRFT typically employs a single fractional order for the spatial domain and another single fractional order for the temporal domain. This restricts their ability to adaptively model heterogeneous features across different vertex clusters, temporal segments, or frequency bands.

Inspired by the concepts of the multiple-parameter GFRFT (MPGFRFT) [25] and multiple-parameter discrete FRFT (MPDFRFT) [26], it is natural to consider introducing multiple fractional orders to control different spectral components, thereby enhancing the expressiveness and adaptability of the transform. However, directly replacing the GFRFT operator in the JFRFT with an MPGFRFT operator is insufficient. Although this modification introduces parameter diversity in the graph spectral domain, it still employs the same set of parameters across the entire temporal dimension, thus failing to fully exploit temporal variability. To effectively capture the spatio-temporal evolution characteristics of dynamic graph signals, it is therefore necessary to design a framework of dynamic multiple-parameter JFRFT (DMPJFRFT) that applies different MPGFRFTs to distinct times within the joint time-vertex fractional spectral domain, enabling a more flexible fractional spectral representation that accounts for the intrinsic characteristics of dynamic graphs.

In GSP, filtering serves as one of the most fundamental and essential operations, enabling noise suppression, signal recovery, and feature enhancement through spectral domain manipulation [11], [14], [17], [20], [27]–[29]. However, fil-

tering dynamic graph signals remains challenging due to their complex and time-varying structures. The proposed DMPJFRFT framework provides a new opportunity to perform adaptive filtering in the joint time-vertex fractional spectral domain, where varying fractional orders enable dynamic graph structure to be effectively modeled in the graph spectral representation. This flexibility facilitates improved filtering performance, including enhanced denoising and deblurring of dynamic graph signals.

The main contributions of this paper are summarized as follows:

- We propose four variants of the DMPJFRFT and establish their theoretical framework for effectively modeling dynamic graph signals.
- We develop a gradient descent-based DMPJFRFT filtering method for effective signal filtering, including denoising and deblurring.
- We introduce a neural network-based DMPJFRFT filtering approach that leverages partial prior information to achieve adaptive filtering with enhanced performance and generalization capabilities.

The remainder of this paper is organized as follows. Section II introduces some necessary preliminary knowledge. Section III presents the four variants of DMPJFRFT along with their theoretical framework. Section IV proposes the gradient descent-based DMPJFRFT filtering method and presents the corresponding simulation results. Section V introduces the neural network-based DMPJFRFT filtering approach and presents its simulation results. Section VI concludes the paper. To provide a clear overview of the proposed framework and its key components, the overall structure of this study is illustrated in Fig. 1. All the technical proofs of our theoretical results are relegated to the Appendix parts.

## II. PRELIMINARIES

### A. Joint Time-Vertex Fractional Fourier Transform

Let  $\mathcal{G} = \{\mathcal{N}, \mathcal{E}, \mathbf{A}\}$  denote a graph with vertex set  $\mathcal{N}$  of cardinality  $|\mathcal{N}| = N$ , and adjacency matrix  $\mathbf{A} \in \mathbb{R}^{N \times N}$ . A static graph signal is represented by  $\mathbf{x} = [x_0, x_1, \dots, x_{N-1}]^T \in \mathbb{C}^N$ , where  $x_i$  denotes the signal value at the  $i$ -th node.

Let  $\mathbf{Z}$  be a graph shift operator (GSO) (e.g., adjacency, Laplacian, normalized Laplacian, row normalized adjacency, or symmetric normalized adjacency) with Jordan decomposition  $\mathbf{Z} = \mathbf{U}_Z \mathbf{J}_Z \mathbf{U}_Z^{-1}$ . The GFT matrix is defined as  $\mathbf{F}_G = \mathbf{U}_Z^{-1}$ , which admits the spectral decomposition  $\mathbf{F}_G = \mathbf{V}_G \mathbf{\Lambda}_G \mathbf{V}_G^{-1}$ . The GFRFT matrix of order  $\alpha \in \mathbb{R}$  is then defined as

$$\mathbf{F}_G^\alpha = \mathbf{V}_G \mathbf{\Lambda}_G^\alpha \mathbf{V}_G^{-1}. \quad (1)$$

This matrix reduces to the identity matrix  $\mathbf{I}_N$  for  $\alpha = 0$  and to the GFT matrix  $\mathbf{F}_G$  for  $\alpha = 1$ .

The DFRFT matrix of order  $\beta$  is

$$\mathbf{D}_T^\beta = \mathbf{V}_T \mathbf{\Lambda}_T^\beta \mathbf{V}_T^{-1}, \quad (2)$$

where  $\mathbf{V}_T$  and  $\mathbf{\Lambda}_T$  are the eigenvectors and eigenvalues of the DFT matrix  $\mathbf{D}_T$ , respectively. Likewise,  $\beta = 0$  yields the identity matrix  $\mathbf{I}_N$  and  $\beta = 1$  recovers the DFT matrix  $\mathbf{D}_T$ .

For a time-varying graph signal  $\mathbf{X} = [\mathbf{x}_1, \dots, \mathbf{x}_T] \in \mathbb{C}^{N \times T}$ , where  $N$  and  $T$  denote the numbers of vertices and time instances, respectively, the JFRFT of  $\mathbf{X}$  with order pair  $(\alpha, \beta) \in \mathbb{R}^2$  is defined as [20], [21]

$$\text{JFRFT}_G^{(\alpha, \beta)}(\mathbf{X}) = \mathbf{F}_G^\alpha \mathbf{X} \left( \mathbf{D}_T^\beta \right)^T. \quad (3)$$

The JFRFT provides a parametric transformation between the time-vertex domain and the joint spectral domain, where the parameters  $(\alpha, \beta)$  control the fractional progression between the identity transform and the full joint Fourier transform. When  $(\alpha, \beta) = (0, 0)$ , the transform reduces to the identity operator, whereas  $(\alpha, \beta) = (1, 1)$  yields the JFT.

For the vectorized signal  $\mathbf{x} = \text{vec}(\mathbf{X}) \in \mathbb{C}^{NT}$ , the JFRFT can be equivalently expressed in matrix form as

$$\text{JFRFT}_G^{(\alpha, \beta)}(\mathbf{x}) = \mathbf{F}_J^{(\alpha, \beta)} \mathbf{x} = \left( \mathbf{D}_T^\beta \otimes \mathbf{F}_G^\alpha \right) \mathbf{x}, \quad (4)$$

where  $\otimes$  denotes the Kronecker product and  $\mathbf{F}_J^{(\alpha, \beta)}$  is JFRFT matrix.

### B. Multiple-Parameter Graph Fractional Fourier Transform

Suppose that  $\mathbf{F}_G$  can be orthogonally decomposed that  $\mathbf{F}_G = \mathbf{V}_G \mathbf{\Lambda}_G \mathbf{V}_G^{-1}$ , where  $\mathbf{V}_G$  is the matrix of eigenvectors and  $\mathbf{\Lambda}_G = \text{diag}(\lambda_0, \dots, \lambda_{N-1})$  is the corresponding eigenvalue matrix. For an order vector  $\mathbf{a} = [a_0, a_1, \dots, a_{N-1}]^T \in \mathbb{R}^N$ , the multiple-parameter GFRFT (MPGFRFT) allows each graph spectral component to be modulated by an individual fractional order parameter. Two alternative forms of MPGFRFT are defined in [25].

The type-I MPGFRFT (MPGFRFT-I) of a graph signal  $\mathbf{x} \in \mathbb{C}^N$  is defined as

$$\hat{\mathbf{x}}_a^I = \mathbf{F}_I^a \mathbf{x}, \quad (5)$$

where

$$\mathbf{F}_I^a = \mathbf{V}_G \text{diag}(\lambda_0^{a_0}, \dots, \lambda_{N-1}^{a_{N-1}}) \mathbf{V}_G^{-1} \quad (6)$$

is the MPGFRFT-I matrix.

The type-II MPGFRFT (MPGFRFT-II) of a graph signal  $\mathbf{x} \in \mathbb{C}^N$  is defined as

$$\hat{\mathbf{x}}_a^{II} = \mathbf{F}_{II}^a \mathbf{x}, \quad (7)$$

$$\mathbf{F}_{II}^a = \sum_{n=0}^{N-1} C_{n, a_n}^{\text{II}} \mathbf{F}_G^n, \quad (8)$$

where  $\mathbf{F}_G$  denotes the GFT matrix and the coefficients are

$$C_{n, a_n}^{\text{II}} = \sum_{j=0}^{N-1} p_{n+1, j+1} \lambda_j^{a_n}, \quad (9)$$

with  $p_{n+1, j+1}$  being the  $(n+1, j+1)$ -th entry of the inverse Vandermonde matrix associated with  $(\lambda_0, \dots, \lambda_{N-1})$ , that is

$$\mathbf{P} = (p_{ij}) \triangleq \begin{pmatrix} 1 & \lambda_0 & \dots & \lambda_0^{N-1} \\ 1 & \lambda_1 & \dots & \lambda_1^{N-1} \\ \vdots & \vdots & \ddots & \vdots \\ 1 & \lambda_{N-1} & \dots & \lambda_{N-1}^{N-1} \end{pmatrix}^{-1}. \quad (10)$$

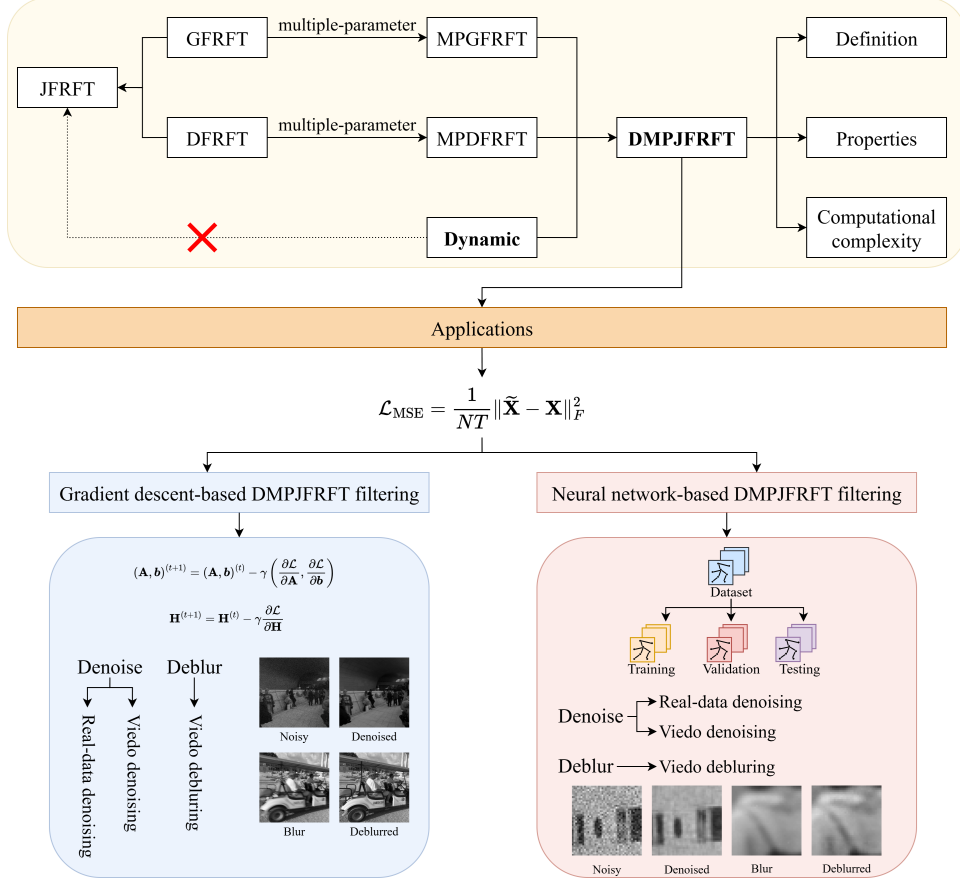


Fig. 1. Overall framework of the proposed DMPJFRFT-based dynamic graph signal processing model.

### C. Multiple-Parameter Discrete Fractional Fourier Transform

For temporal signal  $\mathbf{x} = (x_0, x_1, \dots, x_{T-1})^T \in \mathbb{C}^T$ , classical spectral analysis is usually carried out via the DFRFT. In [26], two types of multiple-parameter DFRFT (MPDFRFT) were proposed, in which each spectral mode is assigned an independent fractional order.

Let  $\mathbf{D}_T$  be a  $T \times T$  DFT matrix, with spectral decomposition  $\mathbf{F}_T = \mathbf{V}_T \mathbf{\Lambda}_T \mathbf{V}_T^H$ , where  $\mathbf{V}_T$  is the matrix of eigenvectors and  $\mathbf{\Lambda}_T = \text{diag}(\mu_0, \dots, \mu_{T-1})$  is the corresponding eigenvalue matrix. The type-I MPDFRFT (MPDFRFT-I) matrix with an order vector  $\mathbf{a} \in \mathbb{R}^T$  is expressed as

$$\mathbf{D}_T^{\mathbf{a}} = \mathbf{V}_T \text{diag}(\mu_0^{a_0}, \dots, \mu_{T-1}^{a_{T-1}}) \mathbf{V}_T^{-1}. \quad (11)$$

The type-II MPDFRFT (MPDFRFT-II) matrix is defined as a linear combination of powers of  $\mathbf{K} = \mathbf{D}_T^{\frac{1}{4}}$

$$\mathbf{D}_{II}^{\mathbf{a}} = \sum_{t=0}^{T-1} D_{t,a_t}^{\text{II}} \mathbf{K}^t, \quad (12)$$

where the coefficients  $D_{t,a_t}^{\text{II}}$  are

$$D_{t,a_t}^{\text{II}} = \frac{1}{T} \frac{1 - e^{j2\pi(t-\frac{T}{4}a_t)}}{1 - e^{j\frac{2\pi}{T}(t-\frac{T}{4}a_t)}}. \quad (13)$$

### III. MULTIPLE-PARAMETER JOINT TIME-VERTEX FRACTIONAL FOURIER TRANSFORM

#### A. Definitions

The JFRFT employs a single fractional order  $\alpha$  for the GFRFT and a single order  $\beta$  for the DFRFT. While this formulation provides a joint spectral representation of time-varying graph signals, it is restricted to a one-parameter family along each dimension, thereby limiting the flexibility of the transform. Consequently, the JFRFT may be insufficient to capture the complex spectral characteristics that evolve over time in graph-structured data.

To overcome this limitation, we can extend the JFRFT by introducing multiple-parameter fractional orders in both the vertex and temporal dimensions. This enables the transform to adaptively characterize distinct spectral behaviors at different time instants by applying different MPGFRFTs to the graph signals corresponding to each moment. Depending on the choice of type-I or type-II operators for the vertex and temporal dimensions, this construction naturally leads to four variants of the DMPJFRFT.

Consider a time-varying graph signal  $\mathbf{X} = [\mathbf{x}_1, \dots, \mathbf{x}_T] \in \mathbb{C}^{N \times T}$ . Let  $\mathbf{A} = [\mathbf{a}^{(1)}, \mathbf{a}^{(2)}, \dots, \mathbf{a}^{(T)}] \in \mathbb{R}^{N \times T}$  denote the matrix of MPGFRFT orders, where  $\mathbf{a}^{(i)} = (a_0^{(i)}, a_1^{(i)}, \dots, a_{N-1}^{(i)})^T \in \mathbb{R}^N$  is the order vector applied to the  $i$ -th column  $\mathbf{x}_i$  of  $\mathbf{X}$  for  $i = 1, 2, \dots, T$ . Similarly, let  $\mathbf{b} = (b_0, b_1, \dots, b_{T-1})^T \in \mathbb{R}^T$  be the fractional order vector

associated with the MPDFRFT along the temporal dimension. For these fractional order parameters  $(\mathbf{A}, \mathbf{b})$ , we can define four types of DMPJFRFT.

*Definition 1:* The type-I-I DMPJFRFT (DMPJFRFT-I-I) of  $\mathbf{X}$  is defined as

$$\begin{aligned} & \text{DMPJFRFT}_{\text{I},\text{I}}^{(\mathbf{A},\mathbf{b})}(\mathbf{X}) \\ &= \left[ \mathbf{F}_{\text{I}}^{\mathbf{a}^{(1)}} \mathbf{x}_1, \mathbf{F}_{\text{I}}^{\mathbf{a}^{(2)}} \mathbf{x}_2, \dots, \mathbf{F}_{\text{I}}^{\mathbf{a}^{(T)}} \mathbf{x}_T \right] (\mathbf{D}_{\text{I}}^{\mathbf{b}})^T. \end{aligned} \quad (14)$$

*Definition 2:* The type-I-II DMPJFRFT (DMPJFRFT-I-II) of  $\mathbf{X}$  is defined as

$$= \left[ \mathbf{F}_{\text{I}}^{\mathbf{a}^{(1)}} \mathbf{x}_1, \mathbf{F}_{\text{I}}^{\mathbf{a}^{(2)}} \mathbf{x}_2, \dots, \mathbf{F}_{\text{I}}^{\mathbf{a}^{(T)}} \mathbf{x}_T \right] (\mathbf{D}_{\text{II}}^{\mathbf{b}})^T. \quad (15)$$

*Definition 3:* The type-II-I DMPJFRFT (DMPJFRFT-II-I) of  $\mathbf{X}$  is defined as

$$\begin{aligned} & \text{DMPJFRFT}_{\text{II},\text{I}}^{(\mathbf{A},\mathbf{b})}(\mathbf{X}) \\ &= \left[ \mathbf{F}_{\text{II}}^{\mathbf{a}^{(1)}} \mathbf{x}_1, \mathbf{F}_{\text{II}}^{\mathbf{a}^{(2)}} \mathbf{x}_2, \dots, \mathbf{F}_{\text{II}}^{\mathbf{a}^{(T)}} \mathbf{x}_T \right] (\mathbf{D}_{\text{I}}^{\mathbf{b}})^T. \end{aligned} \quad (16)$$

*Definition 4:* The type-II-II DMPJFRFT (DMPJFRFT-II-II) of  $\mathbf{X}$  is defined as

$$\begin{aligned} & \text{DMPJFRFT}_{\text{II},\text{II}}^{(\mathbf{A},\mathbf{b})}(\mathbf{X}) \\ &= \left[ \mathbf{F}_{\text{II}}^{\mathbf{a}^{(1)}} \mathbf{x}_1, \mathbf{F}_{\text{II}}^{\mathbf{a}^{(2)}} \mathbf{x}_2, \dots, \mathbf{F}_{\text{II}}^{\mathbf{a}^{(T)}} \mathbf{x}_T \right] (\mathbf{D}_{\text{II}}^{\mathbf{b}})^T. \end{aligned} \quad (17)$$

Let  $\mathbf{x} = \text{vec}(\mathbf{X}) \in \mathbb{C}^{NT}$  be the column-stacked vectorization of  $\mathbf{X}$ . Define the block-diagonal MPGFRFT matrix as

$$\mathbf{F}_{\text{blk},G_{\text{type}}}^{\mathbf{A}} = \text{blkdiag} \left( \mathbf{F}_{G_{\text{type}}}^{\mathbf{a}^{(1)}}, \mathbf{F}_{G_{\text{type}}}^{\mathbf{a}^{(2)}}, \dots, \mathbf{F}_{G_{\text{type}}}^{\mathbf{a}^{(T)}} \right) \quad (18)$$

where  $G_{\text{type}}$  specifies the MPGFRFT type (I or II), and  $\mathbf{F}_{\text{blk},G_{\text{type}}}^{\mathbf{A}} \in \mathbb{C}^{NT \times NT}$ . Then, the four types of DMPJFRFT can be equivalently written in compact vectorized form as

$$\text{DMPJFRFT}_{G_{\text{type}},D_{\text{type}}}^{(\mathbf{A},\mathbf{b})}(\mathbf{x}) = \mathbf{F}_{J,G_{\text{type}},D_{\text{type}}}^{(\mathbf{A},\mathbf{b})} \mathbf{x}, \quad (19)$$

where

$$\mathbf{F}_{J,G_{\text{type}},D_{\text{type}}}^{(\mathbf{A},\mathbf{b})} = \left( \mathbf{D}_{D_{\text{type}}}^{\mathbf{b}} \otimes \mathbf{I}_N \right) \mathbf{F}_{\text{blk},G_{\text{type}}}^{\mathbf{A}} \quad (20)$$

is the DMPJFRFT matrix, and  $D_{\text{type}}$  denotes the chosen MPDFRFT type (I or II).

*Remark 1:* It is worth noting that the proposed DMPJFRFT framework is not merely a multiple-parameter extension of the conventional JFRFT. Its core idea is to apply a distinct set of fractional parameters to each time step of a dynamic graph signal, taking into account the temporal variations inherent in dynamic graph signals, and effectively modeling the signal in the graph spectral domain at each moment. By using different fractional parameters across time, the underlying graph spectral representation evolves dynamically, capturing temporal changes in the graph structure. In this way, DMPJFRFT achieves adaptive time-varying graph structure modeling in the multiple-parameter spectral domain, providing a faithful and flexible representation of dynamic graph signals. To provide an intuitive understanding, Fig. 2 illustrates the overall mechanism of the proposed DMPJFRFT framework.

## B. Properties

*Property 1 (Identity transform):* If the fractional order parameters are set to  $(\mathbf{A}, \mathbf{b}) = (\mathbf{0}_{N \times T}, \mathbf{0}_{T \times 1})$ , then all four types of DMPJFRFT reduce to the identity transform.

*Property 2 (Reduction to JFRFT):* If the fractional order parameters are set to  $(\mathbf{A}, \mathbf{b}) = (\mathbf{a}_{N \times T}, \mathbf{b}_{T \times 1})$ , then all four types of DMPJFRFT reduce to the JFRFT.

*Property 3 (Reduction to JFT):* If the fractional order parameters are set to  $(\mathbf{A}, \mathbf{b}) = (\mathbf{1}_{N \times T}, \mathbf{1}_{T \times 1})$ , then all four types of DMPJFRFT reduce to the JFT.

*Proof:* The proofs of properties 1–3 are straightforward and thus omitted here.

*Property 4 (Index additivity):* Let  $(\mathbf{A}_1, \mathbf{b}_1)$  and  $(\mathbf{A}_2, \mathbf{b}_2)$  be two sets of fractional order parameters, where  $\mathbf{A}_1 = [\mathbf{a}_1^{(1)}, \mathbf{a}_1^{(2)}, \dots, \mathbf{a}_1^{(T)}]$  and  $\mathbf{A}_2 = [\mathbf{a}_2^{(1)}, \mathbf{a}_2^{(2)}, \dots, \mathbf{a}_2^{(T)}]$ . If the MPGFRFT orders in  $\mathbf{A}_2$  are time-invariant, i.e.  $\mathbf{a}_2^{(1)} = \mathbf{a}_2^{(2)} = \dots = \mathbf{a}_2^{(T)}$ , and both the MPGFRFT matrices  $\mathbf{F}_{G_{\text{type}}}^{\mathbf{a}_2^{(r)}}$  and the MPDFRFT matrices  $\mathbf{D}_{D_{\text{type}}}^{\mathbf{b}_r}$  ( $r = 1, 2$ ) satisfy the index additivity property, then the DMPJFRFT satisfies the additivity property that

$$\begin{aligned} & \text{DMPJFRFT}_{G_{\text{type}},D_{\text{type}}}^{(\mathbf{A}_2,\mathbf{b}_2)} \left( \text{DMPJFRFT}_{G_{\text{type}},D_{\text{type}}}^{(\mathbf{A}_1,\mathbf{b}_1)}(\mathbf{X}) \right) \\ &= \text{DMPJFRFT}_{G_{\text{type}},D_{\text{type}}}^{(\mathbf{A}_1+\mathbf{A}_2,\mathbf{b}_1+\mathbf{b}_2)}(\mathbf{X}). \end{aligned} \quad (21)$$

*Proof:* According to (20), we have

$$\begin{aligned} & \mathbf{F}_{J,G_{\text{type}},D_{\text{type}}}^{(\mathbf{A}_2,\mathbf{b}_2)} \mathbf{F}_{J,G_{\text{type}},D_{\text{type}}}^{(\mathbf{A}_1,\mathbf{b}_1)} \\ &= \left( \mathbf{D}_{D_{\text{type}}}^{\mathbf{b}_2} \otimes \mathbf{I}_N \right) \mathbf{F}_{\text{blk},G_{\text{type}}}^{\mathbf{A}_2} \left( \mathbf{D}_{D_{\text{type}}}^{\mathbf{b}_1} \otimes \mathbf{I}_N \right) \mathbf{F}_{\text{blk},G_{\text{type}}}^{\mathbf{A}_1}. \end{aligned} \quad (22)$$

If  $\mathbf{a}_2^{(1)} = \mathbf{a}_2^{(2)} = \dots = \mathbf{a}_2^{(T)}$ , the above equation can be written as

$$\begin{aligned} & \mathbf{F}_{J,G_{\text{type}},D_{\text{type}}}^{(\mathbf{A}_2,\mathbf{b}_2)} \mathbf{F}_{J,G_{\text{type}},D_{\text{type}}}^{(\mathbf{A}_1,\mathbf{b}_1)} \\ &= \left( \mathbf{D}_{D_{\text{type}}}^{\mathbf{b}_2} \otimes \mathbf{I}_N \right) \left( \mathbf{D}_{D_{\text{type}}}^{\mathbf{b}_1} \otimes \mathbf{I}_N \right) \mathbf{F}_{\text{blk},G_{\text{type}}}^{\mathbf{A}_2} \mathbf{F}_{\text{blk},G_{\text{type}}}^{\mathbf{A}_1} \\ &= \left( \mathbf{D}_{D_{\text{type}}}^{\mathbf{b}_2} \mathbf{D}_{D_{\text{type}}}^{\mathbf{b}_1} \otimes \mathbf{I}_N \right) \mathbf{F}_{\text{blk},G_{\text{type}}}^{\mathbf{A}_2} \mathbf{F}_{\text{blk},G_{\text{type}}}^{\mathbf{A}_1}. \end{aligned} \quad (23)$$

It is obvious that

$$\begin{aligned} & \mathbf{F}_{\text{blk},G_{\text{type}}}^{\mathbf{A}_2} \mathbf{F}_{\text{blk},G_{\text{type}}}^{\mathbf{A}_1} \\ &= \text{blkdiag} \left( \mathbf{F}_{G_{\text{type}}}^{\mathbf{a}_2^{(1)}} \mathbf{F}_{G_{\text{type}}}^{\mathbf{a}_1^{(1)}}, \mathbf{F}_{G_{\text{type}}}^{\mathbf{a}_2^{(2)}} \mathbf{F}_{G_{\text{type}}}^{\mathbf{a}_1^{(2)}}, \dots, \mathbf{F}_{G_{\text{type}}}^{\mathbf{a}_2^{(T)}} \mathbf{F}_{G_{\text{type}}}^{\mathbf{a}_1^{(T)}} \right), \end{aligned} \quad (24)$$

thus, if both the MPGFRFT matrices  $\mathbf{F}_{G_{\text{type}}}^{\mathbf{a}_r^{(i)}}$  and the MPDFRFT matrices  $\mathbf{D}_{D_{\text{type}}}^{\mathbf{b}_r}$  ( $r = 1, 2$ ) satisfy the index additivity property, we arrive the required result.  $\square$

*Property 5 (Reversibility):* If each MPGFRFT matrix  $\mathbf{F}_{G_{\text{type}}}^{\mathbf{a}_r^{(i)}}$  ( $i = 1, 2, \dots, T$ ) and the MPDFRFT matrix  $\mathbf{D}_{D_{\text{type}}}^{\mathbf{b}_r}$  are invertible, the DMPJFRFT is invertible. The inverse DMPJFRFT matrix is given by

$$\left( \mathbf{F}_{J,G_{\text{type}},D_{\text{type}}}^{(\mathbf{A},\mathbf{b})} \right)^{-1} = \left( \mathbf{F}_{\text{blk},G_{\text{type}}}^{\mathbf{A}} \right)^{-1} \left( \left( \mathbf{D}_{D_{\text{type}}}^{\mathbf{b}} \right)^{-1} \otimes \mathbf{I}_N \right). \quad (25)$$

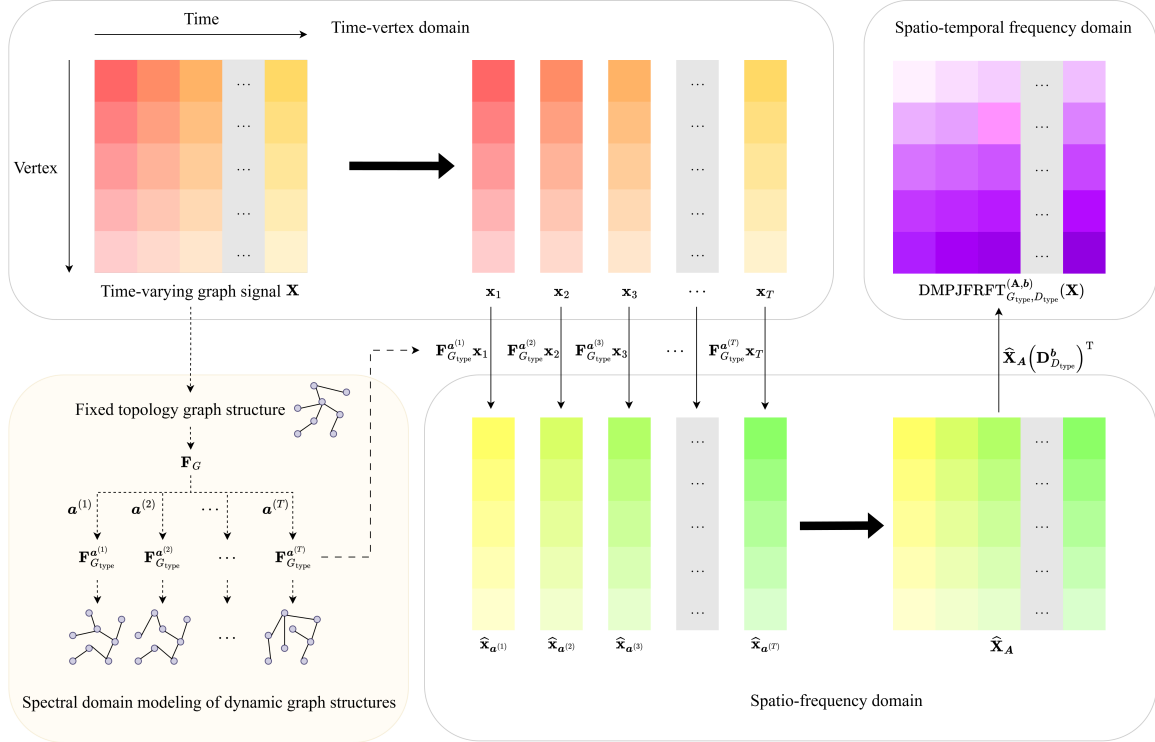


Fig. 2. Conceptual illustration of the DMPJFRFT mechanism.

In particular, for the DMPJFRFT-I-I case, we have

$$\left(\mathbf{F}_{J,I,I}^{(\mathbf{A},\mathbf{b})}\right)^{-1} = \mathbf{F}_{J,I,I}^{(-\mathbf{A},-\mathbf{b})}. \quad (26)$$

*Proof:* If each MPGFRFT matrix  $\mathbf{F}_{G_{\text{type}}}^{\mathbf{a}^{(i)}}$  ( $i = 1, 2, \dots, T$ ) are invertible, the block-diagonal MPGFRFT matrix is invertible

$$\left(\mathbf{F}_{\text{blk},G_{\text{type}}}^{\mathbf{A}}\right)^{-1} = \text{blkdiag}\left(\left(\mathbf{F}_{G_{\text{type}}}^{\mathbf{a}^{(1)}}\right)^{-1}, \dots, \left(\mathbf{F}_{G_{\text{type}}}^{\mathbf{a}^{(T)}}\right)^{-1}\right). \quad (27)$$

If the MPDFRFT matrix  $\mathbf{D}_{D_{\text{type}}}^{\mathbf{b}}$  is invertible, we have

$$\left(\mathbf{D}_{D_{\text{type}}}^{\mathbf{b}} \otimes \mathbf{I}_N\right)^{-1} = \left(\mathbf{D}_{D_{\text{type}}}^{\mathbf{b}}\right)^{-1} \otimes \mathbf{I}_N. \quad (28)$$

In particular, if  $G_{\text{type}} = \mathbf{I}$  and  $D_{\text{type}} = \mathbf{I}$ , we have

$$\begin{aligned} \left(\mathbf{F}_{\text{blk},G_{\text{type}}}^{\mathbf{A}}\right)^{-1} &= \text{blkdiag}\left(\mathbf{F}_{G_{\text{type}}}^{-\mathbf{a}^{(1)}}, \dots, \mathbf{F}_{G_{\text{type}}}^{-\mathbf{a}^{(T)}}\right) \\ &= \mathbf{F}_{\text{blk},G_{\text{type}}}^{-\mathbf{A}}, \end{aligned} \quad (29)$$

$$\left(\mathbf{D}_{D_{\text{type}}}^{\mathbf{b}} \otimes \mathbf{I}_N\right)^{-1} = \mathbf{D}_{D_{\text{type}}}^{-\mathbf{b}} \otimes \mathbf{I}_N. \quad (30)$$

Thus, we arrive the required results.  $\square$

*Property 6 (Index commutativity):* Let  $(\mathbf{A}_1, \mathbf{b}_1)$  and  $(\mathbf{A}_2, \mathbf{b}_2)$  be two sets of fractional order parameters. If the MPDFRFT matrices are commutative, i.e.  $\mathbf{D}_{D_{\text{type}}}^{b_1} \mathbf{D}_{D_{\text{type}}}^{b_2} = \mathbf{D}_{D_{\text{type}}}^{b_2} \mathbf{D}_{D_{\text{type}}}^{b_1}$ , the MPGFRFT orders in  $\mathbf{A}_1$  and  $\mathbf{A}_2$  are time-invariant and the single-block MPGFRFT matrices are

commutative, i.e.  $\mathbf{F}_{G_{\text{type}}}^{a_1^{(1)}} \mathbf{F}_{G_{\text{type}}}^{a_2^{(1)}} = \mathbf{F}_{G_{\text{type}}}^{a_2^{(1)}} \mathbf{F}_{G_{\text{type}}}^{a_1^{(1)}}$ , then the corresponding DMPJFRFT satisfies the commutativity property that

$$\begin{aligned} &\text{DMPJFRFT}_{G_{\text{type}}, D_{\text{type}}}^{(\mathbf{A}_2, \mathbf{b}_2)} \text{DMPJFRFT}_{G_{\text{type}}, D_{\text{type}}}^{(\mathbf{A}_1, \mathbf{b}_1)} \\ &= \text{DMPJFRFT}_{G_{\text{type}}, D_{\text{type}}}^{(\mathbf{A}_1, \mathbf{b}_1)} \text{DMPJFRFT}_{G_{\text{type}}, D_{\text{type}}}^{(\mathbf{A}_2, \mathbf{b}_2)}. \end{aligned} \quad (31)$$

*Proof:* Under the time-invariance assumption, each block-diagonal matrix can be written in Kronecker form as

$$\mathbf{F}_{\text{blk},G_{\text{type}}}^{\mathbf{A}_1} = \mathbf{I}_T \otimes \mathbf{F}_{G_{\text{type}}}^{a_1^{(1)}}, \quad \mathbf{F}_{\text{blk},G_{\text{type}}}^{\mathbf{A}_2} = \mathbf{I}_T \otimes \mathbf{F}_{G_{\text{type}}}^{a_2^{(1)}}. \quad (32)$$

Then, we have

$$\begin{aligned} &\mathbf{F}_J^{(\mathbf{A}_2, \mathbf{b}_2)} \mathbf{F}_J^{(\mathbf{A}_1, \mathbf{b}_1)} \\ &= \left(\mathbf{D}_{D_{\text{type}}}^{b_2} \otimes \mathbf{I}_N\right) \left(\mathbf{I}_T \otimes \mathbf{F}_G^{a_2^{(1)}}\right) \left(\mathbf{D}_{D_{\text{type}}}^{b_1} \otimes \mathbf{I}_N\right) \\ &\quad \times \left(\mathbf{I}_T \otimes \mathbf{F}_G^{a_1^{(1)}}\right) \\ &= \left(\mathbf{D}_{D_{\text{type}}}^{b_2} \mathbf{D}_{D_{\text{type}}}^{b_1}\right) \otimes \left(\mathbf{F}_G^{a_2^{(1)}} \mathbf{F}_G^{a_1^{(1)}}\right). \end{aligned} \quad (33)$$

Since the MPDFRFT and single-block MPGFRFT matrices are assumed to be commutative, i.e.,  $\mathbf{D}_{D_{\text{type}}}^{b_1} \mathbf{D}_{D_{\text{type}}}^{b_2} = \mathbf{D}_{D_{\text{type}}}^{b_2} \mathbf{D}_{D_{\text{type}}}^{b_1}$ ,

$$\mathbf{D}_{D_{\text{type}}}^{b_1} \mathbf{D}_{D_{\text{type}}}^{b_2} = \mathbf{D}_{D_{\text{type}}}^{b_2} \mathbf{D}_{D_{\text{type}}}^{b_1}, \quad (34)$$

$$\mathbf{F}_G^{a_2^{(1)}} \mathbf{F}_G^{a_1^{(1)}} = \mathbf{F}_G^{a_1^{(1)}} \mathbf{F}_G^{a_2^{(1)}}, \quad (35)$$

we arrive the required result.  $\square$

*Property 7 (Linearity):* Let  $\mathbf{X}, \mathbf{Y} \in \mathbb{C}^{N \times T}$  be two time-varying graph signals and  $\alpha, \beta \in \mathbb{C}$ . The DMPJFRFT is linear, i.e.,

$$\begin{aligned} & \text{DMPJFRFT}_{G_{\text{type}}, D_{\text{type}}}^{(\mathbf{A}, \mathbf{b})} (\alpha \mathbf{X} + \beta \mathbf{Y}) \\ &= \alpha \text{DMPJFRFT}_{G_{\text{type}}, D_{\text{type}}}^{(\mathbf{A}, \mathbf{b})} (\mathbf{X}) \\ &+ \beta \text{DMPJFRFT}_{G_{\text{type}}, D_{\text{type}}}^{(\mathbf{A}, \mathbf{b})} (\mathbf{Y}). \end{aligned} \quad (36)$$

*Proof:* Let  $\mathbf{x} = \text{vec}(\mathbf{X})$  and  $\mathbf{y} = \text{vec}(\mathbf{Y})$ . Then, we have

$$\begin{aligned} & \text{DMPJFRFT}_{G_{\text{type}}, D_{\text{type}}}^{(\mathbf{A}, \mathbf{b})} (\alpha \mathbf{X} + \beta \mathbf{Y}) \\ &= \mathbf{F}_{J, G_{\text{type}}, D_{\text{type}}}^{(\mathbf{A}, \mathbf{b})} (\alpha \mathbf{x} + \beta \mathbf{y}) \\ &= \alpha \mathbf{F}_{J, G_{\text{type}}, D_{\text{type}}}^{(\mathbf{A}, \mathbf{b})} \mathbf{x} + \beta \mathbf{F}_{J, G_{\text{type}}, D_{\text{type}}}^{(\mathbf{A}, \mathbf{b})} \mathbf{y}. \end{aligned} \quad (37)$$

Thus, we arrive the required result.  $\square$

### C. Computational complexity

For the the GFRFT and MPGFRFT-I, the main computational cost arises from the spectral decomposition or the computation of fractional powers of the GFT matrix, resulting in a complexity of  $\mathcal{O}(N^3)$ . For the MPGFRFT-II matrix, the matrix powers  $\mathbf{F}_G^n$  can be precomputed, thereby reducing repeated computation during multiple transformations. Thus, the computational complexity of constructing the MPGFRFT-II matrix remains  $\mathcal{O}(N^3)$ . Similarly, the DFRFT and MPDFRFT in the temporal domain require the spectral decomposition or the computation of fractional powers of the DFT matrix, leading to a computational complexity of  $\mathcal{O}(T^3)$ .

For an  $N \times T$  time-varying graph signal  $\mathbf{X}$ , the computational cost of the JFRFT mainly arises from two matrix multiplications involving the graph-domain and temporal-domain fractional transform matrices. Assuming these matrices are precomputed, the overall per-transformation complexity is  $\mathcal{O}(N^2T + NT^2)$ . When  $N \approx T$ , this complexity can be approximated as  $\mathcal{O}(N^3)$ . Therefore, the DMPJFRFT has the same complexity as the conventional JFRFT while providing enhanced spectral flexibility through multi-parameter fractional orders. Table I gives a summary of the computational complexity of the proposed transforms.

TABLE I  
COMPUTATIONAL COMPLEXITY OF DIFFERENT FRACTIONAL TRANSFORMS

Transform	Domain	Complexity
GFRFT	Graph spectral	$\mathcal{O}(N^3)$
MPGFRFT-I	Graph spectral	$\mathcal{O}(N^3)$
MPGFRFT-II	Graph spectral	$\mathcal{O}(N^3)$
DFRFT	Temporal	$\mathcal{O}(T^3)$
MPDFRFT-I	Temporal	$\mathcal{O}(T^3)$
MPDFRFT-II	Temporal	$\mathcal{O}(T^3)$
JFRFT	Joint	$\mathcal{O}(N^2T + NT^2)$
DMPJFRFT	Joint	$\mathcal{O}(N^2T + NT^2)$

## IV. GRADIENT DESCENT-BASED DMPJFRFT FILTERING

The multiple-parameter mechanism enables fine-grained manipulation of the signal representation, which is particularly

beneficial for problems such as denoising and deblurring. In this Section, we develop gradient descent-based filtering schemes in the DMPJFRFT domain.

In this work, we consider two typical signal degradation models: denoising and deblurring, both of which aim to recover the clean time-varying graph signal from its corrupted observation. For the denoising task, the degradation model is given by  $\mathbf{Y} = \mathbf{X} + \mathbf{N}$ , where  $\mathbf{X} \in \mathbb{C}^{N \times T}$  is the pure time-varying graph signal,  $\mathbf{Y}$  is the observed corrupted signal, and  $\mathbf{N}$  represents additive noise. For the deblurring task, the degradation process can be modeled as  $\mathbf{Y} = \mathbf{K}\mathbf{X}$ , where  $\mathbf{K}$  denotes the blurring operator. Regardless of whether the corruption arises from additive noise or blurring, the filtering process in both denoising and deblurring scenarios aims to recover  $\mathbf{X}$  from  $\mathbf{Y}$  by minimizing the mean square error (MSE)

$$\mathcal{L}_{\text{MSE}} = \frac{1}{NT} \|\tilde{\mathbf{X}} - \mathbf{X}\|_F^2, \quad (38)$$

where  $\tilde{\mathbf{X}}$  is the reconstructed signal after filtering. Specifically, the reconstruction process can be expressed as

$$\text{vec}(\tilde{\mathbf{X}}) = \left( \mathbf{F}_{J, G_{\text{type}}, D_{\text{type}}}^{(\mathbf{A}, \mathbf{b})} \right)^{-1} \mathbf{H} \mathbf{F}_{J, G_{\text{type}}, D_{\text{type}}}^{(\mathbf{A}, \mathbf{b})} \mathbf{x}, \quad (39)$$

where  $\mathbf{x} = \text{vec}(\mathbf{X})$  and  $\mathbf{H}$  is the learnable diagonal filter.

Since both the MPGFRFT and MPDFRFT are differentiable with respect to their transform parameters, the DMPJFRFT naturally inherits this property and is therefore differentiable with respect to  $(\mathbf{A}, \mathbf{b})$ . Consequently, gradient descent can be effectively employed to jointly optimize the transform parameters and the spectral filter.

The parameters are updated iteratively by

$$(\mathbf{A}, \mathbf{b})^{(t+1)} = (\mathbf{A}, \mathbf{b})^{(t)} - \gamma \left( \frac{\partial \mathcal{L}}{\partial \mathbf{A}}, \frac{\partial \mathcal{L}}{\partial \mathbf{b}} \right), \quad (40)$$

$$\mathbf{H}^{(t+1)} = \mathbf{H}^{(t)} - \gamma \frac{\partial \mathcal{L}}{\partial \mathbf{H}}, \quad (41)$$

where  $\gamma$  is the learning rate.

Note that for the MPGFRFT-II, the transformation involves the matrix defined  $\mathbf{P}$  in (10). When the modulus of some eigenvalues deviates from one and the number of vertices  $N$  is large, computing  $\mathbf{P}$  may become numerically unstable or even fail due to ill-conditioning. Consequently, in the following experiments, we restrict our attention to DMPJFRFT-I-I and DMPJFRFT-I-II.

To quantitatively evaluate the filtering performance, we adopt the signal-to-noise ratio (SNR), defined as

$$\text{SNR} = 20 \log_{10} \frac{\|\mathbf{X}\|_F}{\|\tilde{\mathbf{X}} - \mathbf{X}\|_F}, \quad (42)$$

Higher SNR values indicate better recovery quality.

### A. Denoising

1) *Real-data denoising:* For graph signal denoising, we use four real-world datasets: PEMSD7(M), PEMSD8, Quality [30]–[32], and SST dataset [33]. For each dataset, the first 30 temporal slices are extracted, and every 10 consecutive

TABLE II  
SNR PERFORMANCE OF GRADIENT DESCENT-BASED DENOISING METHODS UNDER VARIOUS GSOs FOR REAL-WORLD GRAPH SIGNALS.

PEMSD7(M)	$\sigma = 70$ (SNR=-0.446)					$\sigma = 80$ (SNR=-1.606)					$\sigma = 90$ (SNR=-2.629)				
	2D GFRFT	2D GBFRFT	JFRFT	DMPJFRFT-I-I	DMPJFRFT-I-II	2D GFRFT	2D GBFRFT	JFRFT	DMPJFRFT-I-I	DMPJFRFT-I-II	2D GFRFT	2D GBFRFT	JFRFT	DMPJFRFT-I-I	DMPJFRFT-I-II
adj	21.813	22.414	22.246	<b>33.438</b>	23.502	21.128	21.669	<b>33.227</b>	24.355	20.463	20.955	<b>20.816</b>	<b>32.870</b>	24.451	
lap	22.018	22.411	22.419	<b>33.330</b>	25.788	21.287	21.678	<b>33.363</b>	25.503	20.586	20.981	<b>20.899</b>	<b>33.053</b>	24.349	
nor lap	21.888	22.373	22.204	<b>33.206</b>	25.387	21.180	21.671	<b>33.435</b>	25.225	20.499	20.960	<b>20.841</b>	<b>32.815</b>	25.408	
row nor adj	21.854	22.390	22.228	<b>33.259</b>	24.310	21.158	21.649	<b>33.333</b>	24.728	20.481	20.946	<b>20.808</b>	<b>33.227</b>	24.614	
sym nor adj	21.854	22.390	22.228	<b>33.259</b>	24.310	21.158	21.649	<b>33.333</b>	24.728	20.481	20.946	<b>20.808</b>	<b>33.227</b>	24.614	
PEMS08	$\sigma = 80$ (SNR=1.865)					$\sigma = 100$ (SNR=-0.073)					$\sigma = 120$ (SNR=-1.657)				
adj	8.284	8.416	14.294	<b>23.045</b>	18.518	7.190	7.343	13.164	<b>21.917</b>	17.930	6.357	6.520	12.121	<b>22.287</b>	17.656
lap	9.995	10.250	14.249	<b>22.449</b>	19.150	9.277	9.554	13.101	<b>22.588</b>	17.239	8.764	9.382	12.289	<b>21.343</b>	18.345
nor lap	9.659	9.902	14.501	<b>22.746</b>	18.682	8.793	9.042	13.417	<b>22.101</b>	18.613	8.159	8.407	12.525	<b>21.874</b>	17.947
row nor adj	9.888	10.025	14.563	<b>23.085</b>	17.648	9.161	9.311	13.498	<b>22.699</b>	17.072	8.628	8.813	12.613	<b>22.361</b>	17.082
sym nor adj	9.717	9.926	14.523	<b>23.030</b>	18.138	8.845	9.063	13.430	<b>22.809</b>	18.116	8.195	8.426	12.524	<b>22.397</b>	18.703
Quality	$\sigma = 80$ (SNR=2.034)					$\sigma = 90$ (SNR=1.011)					$\sigma = 100$ (SNR=0.095)				
adj	6.776	7.024	12.608	<b>20.540</b>	17.693	6.127	6.374	11.868	<b>20.984</b>	16.648	5.575	5.803	11.187	<b>20.645</b>	15.897
lap	6.913	7.239	12.965	<b>20.604</b>	15.882	6.213	6.578	12.328	<b>21.109</b>	15.069	5.619	6.010	11.754	<b>21.369</b>	15.316
nor lap	6.684	6.925	14.133	<b>21.429</b>	15.636	6.124	6.268	13.594	<b>21.664</b>	15.163	5.550	6.123	13.088	<b>21.617</b>	16.056
row nor adj	7.552	7.593	12.708	<b>16.795</b>	<b>16.911</b>	6.862	9.644	12.001	16.121	<b>17.737</b>	6.263	9.144	11.353	15.866	<b>19.120</b>
sym nor adj	6.234	6.534	12.585	<b>21.381</b>	15.513	5.613	6.163	11.943	<b>21.370</b>	16.339	5.559	9.221	11.292	<b>21.695</b>	17.887
SST	$\sigma = 15$ (SNR=2.987)					$\sigma = 20$ (SNR=0.488)					$\sigma = 25$ (SNR=-1.450)				
adj	12.624	12.793	18.287	<b>29.720</b>	19.467	11.172	11.377	16.804	<b>29.075</b>	19.595	10.105	10.271	15.600	<b>28.101</b>	18.874
lap	15.629	15.843	20.540	<b>30.216</b>	22.953	14.163	14.366	18.997	<b>28.679</b>	21.895	13.040	13.267	17.702	<b>28.517</b>	21.537
nor lap	14.898	15.096	19.548	<b>32.872</b>	22.313	13.623	13.796	18.150	<b>31.844</b>	20.459	12.612	12.805	16.996	<b>22.425</b>	20.146
row nor adj	15.555	15.780	20.518	<b>30.081</b>	21.160	14.109	14.308	19.040	<b>29.733</b>	20.066	12.992	13.203	17.857	<b>28.637</b>	19.451
sym nor adj	14.920	15.109	19.537	<b>29.743</b>	20.708	13.641	13.813	18.142	<b>29.097</b>	21.623	12.629	12.824	16.996	<b>28.842</b>	18.541

columns are regarded as a single time-varying graph signal for filtering. In the experiments, the learning rate is set to 0.01, and the number of training epochs is 1000. The diagonal filter  $\mathbf{H}$  is initialized as an identity matrix, while the transform parameters of the DMPJFRFT are all initialized to 0.5.

We compare the proposed DMPJFRFT-based filtering schemes with three baseline methods: two-dimensional GFRFT (2D GFRFT) [34], 2D graph bi-fractional Fourier transform (2D GBFRFT), and JFRFT. All methods are evaluated under five types of GSOs: the adjacency matrix (adj), the Laplacian (lap), the normalized Laplacian (nor lap), the row-normalized adjacency matrix (row nor adj), and the symmetrically normalized adjacency matrix (sym nor adj). To further assess robustness, experiments are conducted under multiple noise levels controlled by the standard deviation parameter  $\sigma$ . Table II presents the SNR results of these methods across different GSOs and noise levels. The results clearly show that both types of DMPJFRFT-based filters exhibit consistently excellent denoising performance, surpassing all comparison methods across all experimental settings.

2) *Video denoising*: We conduct video denoising experiments using the publicly available REDS dataset [35]. Five representative videos (Video. 08, 09, 11, 27, and 29) are selected for testing. For each sequence, three consecutive frames are extracted to form one time-varying video signal. Each frame is first resized to  $512 \times 512$  pixels and then divided into non-overlapping sub-images of size  $16 \times 16$ . Each sub-image is vectorized and concatenated across the three frames, resulting in a time-varying graph signal of dimension  $256 \times 3$ . We construct a 4-nearest neighbor (4-NN) graph. The filter coefficients are initialized to one, and all learnable parameters are initialized to 0.5. The network is trained for 800 epochs with a learning rate of 0.01. To quantitatively evaluate denoising performance, we adopt three widely used image quality metrics: MSE, peak SNR (PSNR), and structural similarity index (SSIM). The PSNR is defined as

$$\text{PSNR} = 10\log_{10} \left( \frac{255^2}{\text{MSE}} \right). \quad (43)$$

Table III reports the MSE, PSNR, and SSIM results for the five video sequences under  $\sigma = 45$ . The results show that the proposed DMPJFRFT-based denoising schemes consistently outperform the compared methods across all test sequences, demonstrating their superior capability in recovering fine spatial and temporal details.

To further demonstrate the denoising performance, we provide visual comparisons. Fig. 3 shows three consecutive frames from video 29, along with corresponding zoomed-in regions that highlight fine details. From both the full-frame views and the local magnified patches, it can be observed that the DMPJFRFT-based filtering method effectively removes almost all noise while preserving structural details and texture. In contrast, the other three compared methods leave noticeable residual noise points.

### B. Deblurring

The experimental setup for video deblurring is the same as 2) *Video denoising* that described in Section IV-A, using the REDS dataset with paired sharp and blurred frames. Table IV reports the quantitative results for the selected video sequences, showing that the proposed DMPJFRFT-based method consistently outperforms the compared approaches in terms of MSE, PSNR and SSIM.

To further illustrate the restoration quality, Fig. 4 presents the deblurring results for video 11. It can be observed that the proposed DMPJFRFT-based methods (DMPJFRFT-I-I and DMPJFRFT-I-II) and the JFRFT-based method both achieve significantly better visual quality than the 2D GFRFT and 2D GBFRFT, effectively removing blur while preserving edge sharpness and structural details. Notably, the visual results of JFRFT and the two DMPJFRFT variants appear quite similar. This is mainly because, under the current experimental setting where complete prior information of the signal is available, both methods can reconstruct the spatio-temporal frequency structures with high fidelity. However, quantitative evaluation metrics in Table IV still indicate that our proposed methods perform slightly better, suggesting their stronger adaptability.

TABLE III  
DENOISING PERFORMANCE OF GRADIENT DESCENT-BASED METHODS ON FIVE REPRESENTATIVE VIDEOS (VIDEO 08, 09, 11, 27, AND 29) FROM THE REDS DATASET.

Video 08	Frame 1			Frame 2			Frame 3		
	MSE	PSNR	SSIM	MSE	PSNR	SSIM	MSE	PSNR	SSIM
2D GFRFT	$4.865 \times 10^1$	31.260	0.926807	$7.744 \times 10^1$	29.241	0.945602	$4.873 \times 10^1$	31.253	0.934619
2D GBFRFT	$4.891 \times 10^1$	31.237	0.927338	$7.700 \times 10^1$	29.266	0.946263	$4.911 \times 10^1$	31.219	0.934901
JFRFT	$5.449 \times 10^{-1}$	50.768	0.998790	1.848	45.465	0.996414	2.634	43.925	0.995053
DMPJFRFT-I-I	$3.603 \times 10^{-5}$	92.565	<b>1.000000</b>	$5.103 \times 10^{-5}$	91.052	<b>1.000000</b>	$5.880 \times 10^{-5}$	90.437	<b>1.000000</b>
DMPJFRFT-I-II	$5.249 \times 10^{-6}$	<b>100.930</b>	<b>1.000000</b>	$3.862 \times 10^{-6}$	<b>102.263</b>	<b>1.000000</b>	$7.137 \times 10^{-6}$	<b>99.596</b>	<b>1.000000</b>
Video 09	Frame 1			Frame 2			Frame 3		
	MSE	PSNR	SSIM	MSE	PSNR	SSIM	MSE	PSNR	SSIM
2D GFRFT	3.460	42.741	0.986918	4.831	41.291	0.993086	3.549	42.630	0.986919
2D GBFRFT	4.127	41.974	0.986405	4.848	41.276	0.993085	4.141	41.960	0.986415
JFRFT	$2.993 \times 10^{-2}$	63.370	0.999934	$5.282 \times 10^{-2}$	60.903	0.999880	$1.109 \times 10^{-2}$	67.682	0.999963
DMPJFRFT-I-I	$1.013 \times 10^{-5}$	98.075	<b>1.000000</b>	$7.616 \times 10^{-6}$	99.314	<b>1.000000</b>	$8.122 \times 10^{-6}$	99.034	<b>1.000000</b>
DMPJFRFT-I-II	$1.170 \times 10^{-6}$	<b>107.448</b>	<b>1.000000</b>	$5.982 \times 10^{-7}$	<b>110.363</b>	<b>1.000000</b>	$9.282 \times 10^{-7}$	<b>108.455</b>	<b>1.000000</b>
Video 11	Frame 1			Frame 2			Frame 3		
	MSE	PSNR	SSIM	MSE	PSNR	SSIM	MSE	PSNR	SSIM
2D GFRFT	$1.140 \times 10^2$	27.560	0.880162	$1.334 \times 10^2$	26.879	0.916380	$1.141 \times 10^2$	27.556	0.886830
2D GBFRFT	$1.127 \times 10^2$	27.612	0.882048	$1.318 \times 10^2$	26.932	0.917313	$1.128 \times 10^2$	27.608	0.888590
JFRFT	2.034	45.047	0.996583	2.964	43.412	0.995574	3.981	42.131	0.993599
DMPJFRFT-I-I	$7.181 \times 10^{-5}$	89.569	<b>1.000000</b>	$1.344 \times 10^{-4}$	86.847	0.999999	$1.753 \times 10^{-4}$	85.694	0.999999
DMPJFRFT-I-II	$4.109 \times 10^{-6}$	<b>101.993</b>	<b>1.000000</b>	$5.547 \times 10^{-6}$	<b>100.690</b>	<b>1.000000</b>	$1.015 \times 10^{-5}$	<b>98.066</b>	<b>1.000000</b>
Video 27	Frame 1			Frame 2			Frame 3		
	MSE	PSNR	SSIM	MSE	PSNR	SSIM	MSE	PSNR	SSIM
2D GFRFT	$6.107 \times 10^1$	30.273	0.924801	$1.145 \times 10^2$	27.543	0.897960	$6.131 \times 10^1$	30.255	0.925035
2D GBFRFT	$6.020 \times 10^1$	30.334	0.926680	$1.125 \times 10^2$	27.619	0.899891	$5.998 \times 10^1$	30.350	0.927568
JFRFT	$8.758 \times 10^{-1}$	48.707	0.998545	1.973	45.181	0.996993	1.653	45.949	0.997599
DMPJFRFT-I-I	$1.239 \times 10^{-4}$	87.201	0.999999	$2.597 \times 10^{-4}$	83.986	0.999999	$2.497 \times 10^{-4}$	84.156	0.999998
DMPJFRFT-I-II	$3.789 \times 10^{-6}$	<b>102.345</b>	<b>1.000000</b>	$1.610 \times 10^{-5}$	<b>96.062</b>	<b>1.000000</b>	$3.931 \times 10^{-6}$	<b>102.185</b>	<b>1.000000</b>
Video 29	Frame 1			Frame 2			Frame 3		
	MSE	PSNR	SSIM	MSE	PSNR	SSIM	MSE	PSNR	SSIM
2D GBFRFT	9.939	38.157	0.960086	$1.778 \times 10^1$	35.633	0.961815	9.976	38.141	0.962655
2D GFRFT	$1.019 \times 10^1$	38.047	0.957525	$1.791 \times 10^1$	35.600	0.961386	$1.022 \times 10^1$	38.035	0.959982
JFRFT	$1.426 \times 10^{-1}$	56.590	0.999347	$3.919 \times 10^{-1}$	52.199	0.998402	$3.515 \times 10^{-1}$	52.672	0.998605
DMPJFRFT-I-I	$9.221 \times 10^{-5}$	88.483	0.999999	$8.088 \times 10^{-5}$	89.052	0.999999	$1.040 \times 10^{-4}$	87.960	0.999998
DMPJFRFT-I-II	$8.535 \times 10^{-7}$	<b>108.819</b>	<b>1.000000</b>	$8.750 \times 10^{-7}$	<b>108.711</b>	<b>1.000000</b>	$2.428 \times 10^{-6}$	<b>104.278</b>	<b>1.000000</b>

To provide a more detailed comparison, Fig. 5 presents the zoomed-in regions of the second frame, where red rectangles highlight areas with noticeable local details. Although the overall visual appearance of JFRFT, DMPJFRFT-I-I, and DMPJFRFT-I-II is similar, the proposed methods still produce slightly finer texture restoration within these highlighted regions.

## V. NEURAL NETWORK-BASED DMPJFRFT FILTERING

Although the gradient descent-based DMPJFRFT filtering scheme demonstrates strong denoising and deblurring capabilities, it still faces certain limitations in practical applications. Specifically, this method requires complete prior knowledge of the clean signal, which is often unavailable in real-world scenarios. To address this limitation, we propose a neural network-based framework, termed DMPJFRFTNet, which learns to perform filtering with only partial prior information.

In the proposed DMPJFRFTNet, the time-varying graph signals are divided into training, validation, and testing sets. The training and validation sets contain paired clean and corrupted signals, which are used to optimize the learnable

parameters of the network, including the fractional orders and filter coefficients. During testing, however, only corrupted signals are provided, allowing the model to generalize and infer the underlying clean signal without explicit prior knowledge. The overall architecture of the proposed DMPJFRFTNet are illustrated in Fig. 6.

The overall architecture of DMPJFRFTNet integrates the DMPJFRFT as a differentiable fully connected layer within the network. A time-varying graph signal is represented as a matrix  $\mathbf{X} \in \mathbb{C}^{N \times TM}$ , where  $N$  denotes the number of vertices,  $T$  represents the number of time frames for each sample, and  $M$  is the number of signal samples in a batch. Equivalently,  $\mathbf{X}$  can be viewed as  $M$  time-varying graph signals  $\mathbf{X}_1, \mathbf{X}_2, \dots, \mathbf{X}_M$ , each of dimension  $N \times T$ .

Within this framework, the DMPJFRFT transformation module performs a joint spectral representation of each time-varying graph signal. The forward DMPJFRFT layer, implemented as a fully connected operation, transforms  $\mathbf{X}$  into its spectral-domain representation  $\mathbf{Y} = \mathbf{F}_{J, G_{\text{type}}, D_{\text{type}}}^{(\mathbf{A}, \mathbf{b})}(\mathbf{X}) \in \mathbb{C}^{N \times TM}$ , where  $(\mathbf{A}, \mathbf{b})$  are the learnable fractional orders in the graph and temporal dimensions. These parameters are op-

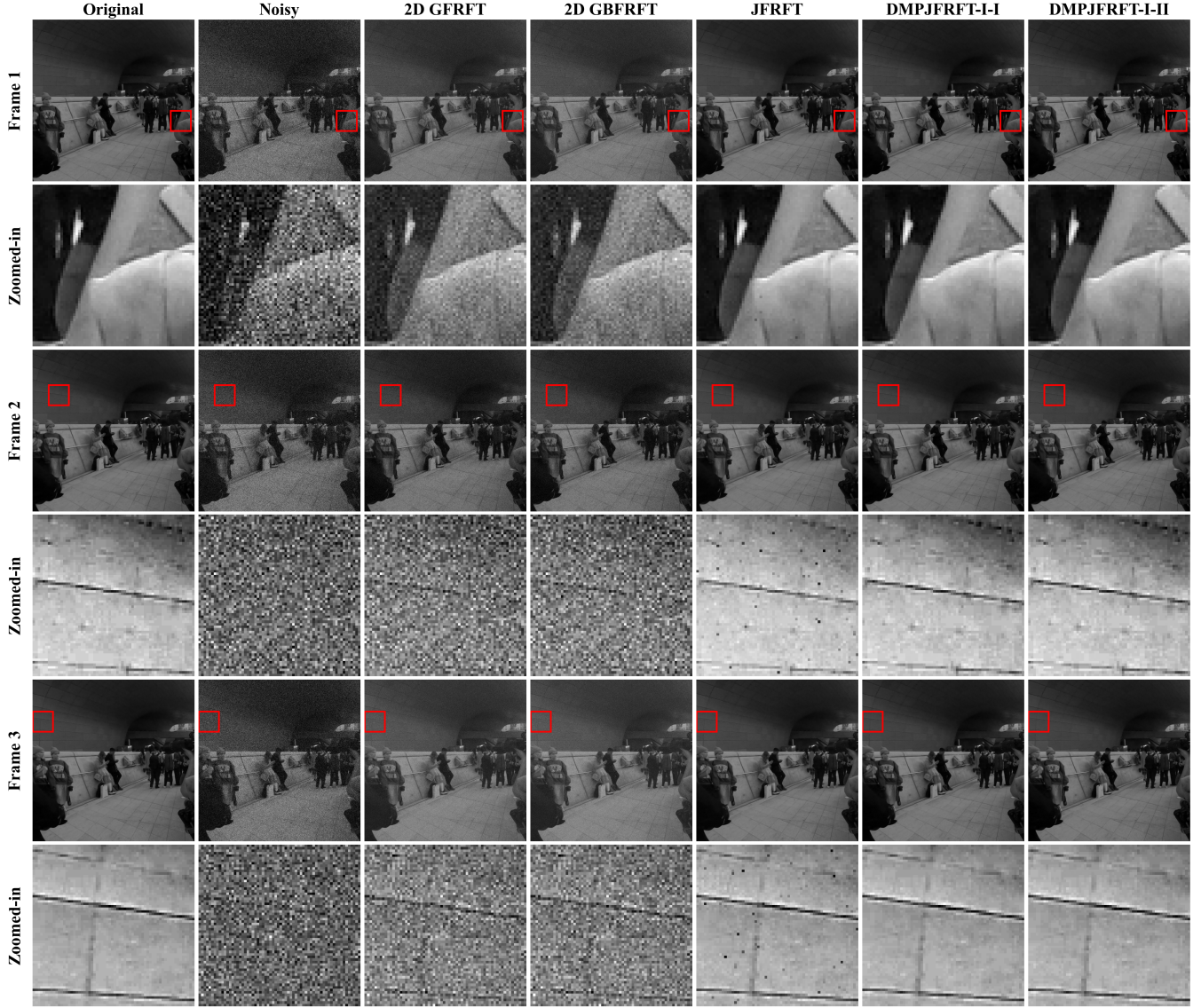


Fig. 3. Visual comparison of denoising results for Video 29.

timized during training, allowing the layer to adaptively adjust the spectral representation to different signal characteristics. In this domain, a learnable diagonal filter  $\mathbf{H}$  enhances meaningful signal components while suppressing noise or blur. Finally, the inverse DMPJFRFT reconstructs the filtered signal back to the vertex domain, yielding the restored time-varying graph signal  $\tilde{\mathbf{X}}$ . The detailed training and inference procedure of DMPJFRFTNet is summarized in Algorithm 1.

#### A. Denoising

1) *Real-data denoising*: We conduct denoising experiments on real-world time-varying graph signals using the same datasets described in Section IV-A. For each dataset, we truncate the first 1500 time series, and treat every 6 consecutive columns as a single time-varying graph signal. From the resulting set, 20% of signals are randomly selected as the test set, while the remaining 80% are split into training and validation sets with a ratio of 8 : 2. The learning rate is set

to 0.001. For the SST dataset, the number of training epochs is set to 100, whereas for the other three datasets, 200 epochs are used. The initial values of the spectral filter coefficients are set to 1, and the initial fractional orders in both graph and temporal dimensions are set to 0.5.

We compare the denoising performance of 2D GFRFTNet, 2D GBFRFTNet, and JFRFTNet under five types of GSOs and different noise levels. The results are summarized in Table V. It can be observed that the proposed DMPJFRFT-based neural network consistently achieves the highest SNR across different GSOs and noise levels.

To further validate the effectiveness of the proposed DMPJFRFT-based models, we select the best results from the five GSOs for each method and compare them with several representative graph neural network approaches, including APPNP [36], ARMAconv [36], BernNet [37], ChebyNet [27], GAT [38], GCN [39], LanczosNet [40], Specformer [41], SpectralCNN [42], [43], and UniMP [44]. The comparison

TABLE IV  
DEBLURING PERFORMANCE OF GRADIENT DESCENT-BASED METHODS ON FIVE REPRESENTATIVE VIDEOS (VIDEO 08, 09, 11, 27, AND 29) FROM THE REDS DATASET.

Video 08	Frame 1			Frame 2			Frame 3		
	MSE	PSNR	SSIM	MSE	PSNR	SSIM	MSE	PSNR	SSIM
2D GFRFT	$4.60 \times 10^{-1}$	31.499	0.934863	$7.45 \times 10^{-1}$	29.406	0.948618	$4.61 \times 10^{-1}$	31.494	0.943404
2D GBFRFT	$4.62 \times 10^{-1}$	31.489	0.932986	$7.47 \times 10^{-1}$	29.395	0.948470	$4.61 \times 10^{-1}$	31.492	0.941310
JFRFT	$2.28 \times 10^{-2}$	64.553	0.999911	$7.36 \times 10^{-2}$	59.465	0.999827	$1.31 \times 10^{-1}$	56.972	0.999682
DMPJFRFT-I-I	$4.55 \times 10^{-4}$	81.549	0.999998	$8.12 \times 10^{-4}$	79.036	0.999995	$7.85 \times 10^{-4}$	79.181	0.999996
DMPJFRFT-I-II	$1.23 \times 10^{-4}$	<b>87.218</b>	<b>0.999999</b>	$1.03 \times 10^{-4}$	<b>87.996</b>	<b>0.999999</b>	$9.46 \times 10^{-5}$	<b>88.371</b>	<b>0.999999</b>
Video 09	Frame 1			Frame 2			Frame 3		
	MSE	PSNR	SSIM	MSE	PSNR	SSIM	MSE	PSNR	SSIM
2D GFRFT	1.98	45.163	0.996352	4.78	41.333	0.993171	1.98	45.163	0.996344
2D GBFRFT	2.30	44.521	0.993869	4.79	41.324	0.993164	2.29	44.533	0.993918
JFRFT	$6.49 \times 10^{-4}$	80.011	0.999998	$1.05 \times 10^{-3}$	77.932	0.999997	$3.60 \times 10^{-4}$	82.570	0.999998
DMPJFRFT-I-I	$3.28 \times 10^{-4}$	82.972	0.999999	$4.06 \times 10^{-4}$	82.043	0.999998	$4.79 \times 10^{-4}$	81.324	0.999998
DMPJFRFT-I-II	$1.15 \times 10^{-4}$	<b>87.536</b>	<b>0.999999</b>	$5.57 \times 10^{-5}$	<b>90.671</b>	<b>1.000000</b>	$6.55 \times 10^{-5}$	<b>89.971</b>	<b>1.000000</b>
Video 11	Frame 1			Frame 2			Frame 3		
	MSE	PSNR	SSIM	MSE	PSNR	SSIM	MSE	PSNR	SSIM
2D GFRFT	$1.08 \times 10^2$	27.789	0.891081	$1.27 \times 10^2$	27.083	0.920668	$1.08 \times 10^2$	27.788	0.897674
2D GBFRFT	$1.08 \times 10^2$	27.806	0.890285	$1.27 \times 10^2$	27.094	0.920631	$1.08 \times 10^2$	27.807	0.896928
JFRFT	$1.01 \times 10^{-1}$	58.081	0.999861	$1.48 \times 10^{-1}$	56.435	0.999734	$1.91 \times 10^{-1}$	55.310	0.999635
DMPJFRFT-I-I	$4.52 \times 10^{-4}$	81.581	0.999998	$7.05 \times 10^{-4}$	79.647	0.999995	$6.40 \times 10^{-4}$	80.070	0.999997
DMPJFRFT-I-II	$9.74 \times 10^{-5}$	<b>88.247</b>	<b>0.999999</b>	$7.83 \times 10^{-5}$	<b>89.190</b>	<b>0.999999</b>	$8.28 \times 10^{-5}$	<b>88.950</b>	<b>0.999999</b>
Video 27	Frame 1			Frame 2			Frame 3		
	MSE	PSNR	SSIM	MSE	PSNR	SSIM	MSE	PSNR	SSIM
2D GFRFT	$5.74 \times 10^1$	30.538	0.932755	$1.08 \times 10^2$	27.788	0.904006	$5.74 \times 10^1$	30.540	0.933115
2D GBFRFT	$5.73 \times 10^1$	30.551	0.931649	$1.08 \times 10^2$	27.786	0.904105	$5.73 \times 10^1$	30.551	0.932029
JFRFT	$2.96 \times 10^{-2}$	63.415	0.999935	$6.08 \times 10^{-2}$	60.292	0.999877	$9.00 \times 10^{-2}$	58.588	0.999882
DMPJFRFT-I-I	$3.42 \times 10^{-4}$	82.792	0.999998	$6.38 \times 10^{-4}$	80.081	0.999996	$6.17 \times 10^{-4}$	80.228	0.999997
DMPJFRFT-I-II	$5.51 \times 10^{-5}$	<b>90.719</b>	<b>1.000000</b>	$3.50 \times 10^{-5}$	<b>92.686</b>	<b>1.000000</b>	$3.77 \times 10^{-5}$	<b>92.373</b>	<b>1.000000</b>
Video 29	Frame 1			Frame 2			Frame 3		
	MSE	PSNR	SSIM	MSE	PSNR	SSIM	MSE	PSNR	SSIM
2D GFRFT	9.24	38.474	0.965326	$1.72 \times 10^1$	35.785	0.963183	9.24	38.473	0.967920
2D GBFRFT	9.38	38.407	0.963393	$1.71 \times 10^1$	35.792	0.963196	9.39	38.406	0.966096
JFRFT	$5.57 \times 10^{-3}$	70.676	0.999963	$1.96 \times 10^{-2}$	65.214	0.999907	$1.80 \times 10^{-2}$	65.586	0.999927
DMPJFRFT-I-I	$1.98 \times 10^{-4}$	85.161	0.999998	$3.70 \times 10^{-4}$	82.453	0.999996	$3.53 \times 10^{-4}$	82.647	0.999997
DMPJFRFT-I-II	$4.58 \times 10^{-5}$	<b>91.522</b>	<b>1.000000</b>	$2.50 \times 10^{-5}$	<b>94.151</b>	<b>1.000000</b>	$2.27 \times 10^{-5}$	<b>94.564</b>	<b>1.000000</b>

methods are trained with a batch size of 16, and their learning rate and number of epochs are kept consistent with the settings described above to ensure fairness. The denoising results are summarized in Table VI. Except for the Quality dataset, where LanczosNet achieves slightly better denoising performance, the proposed DMPJFRFT-based networks consistently outperform all baseline methods across the remaining datasets.

2) *Video denoising*: The video denoising experiments are conducted using five sequences from the publicly available GoPro dataset [45], namely GOPR0384\_11\_02, GOPR0384\_11\_03, GOPR0869\_11\_00, GOPR0396\_11\_00, and GOPR0385\_11\_01. Each sequence contains 1100 frames, and every consecutive five frames are treated as a short video clip. Each frame is first resized to  $128 \times 128$ , then divided into 64 non-overlapping  $16 \times 16$  patches, each of which is vectorized and represented as a graph signal. A 4-NN graph is constructed for each patch. The noisy videos are generated by adding Gaussian noise with  $\sigma = 45$ . The learning rate is set to 0.001, and the number of training epochs is 500.

We randomly select 20% of the video clips for testing, while the remaining 80% are divided into training and validation sets with a ratio of 8 : 2. Table VII summarizes the average denoising performance of the proposed DMPJFRFTNet along with several representative baseline methods on the test set, evaluated using three standard image quality metrics: MSE, PSNR, and SSIM. The results indicate that DMPJFRFTNet attains the best overall performance, verifying the effectiveness of the proposed multiple-parameter joint fractional transform framework.

To further demonstrate the visual superiority of the proposed model, Fig. 7 shows the denoising results on the 3rd frame of the 19th test sample from the GOPR0869\_11\_00 video sequence. As can be seen, the two DMPJFRFTNet variants yield the most restorations, with the least remaining noise and well-preserved structural details.



Fig. 4. Visual comparison of deblurring results for Video 11.

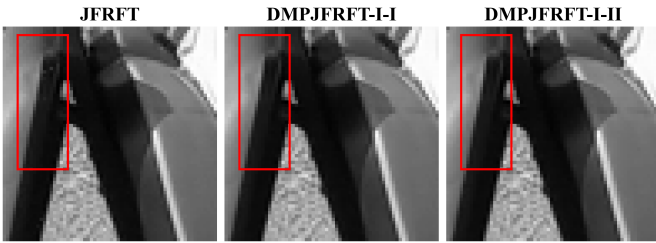


Fig. 5. Zoomed-in comparison of local details in the second frame among JFRFT, DMPJFRFT-I-I, and DMPJFRFT-I-II for Video 08.

### B. Deblurring

In this experiment, the input videos are corrupted by Gaussian blur with kernel size 15, while all other experimental settings remain the same as those in 2) *Video denoising* in Section V-A. Table VIII presents the quantitative comparison results of the proposed DMPJFRFTNet and several repre-

sentative baseline methods in terms of MSE, PSNR, and SSIM, averaged over all video sequences in the test set. The proposed model achieves superior quantitative results, underscoring the benefit of the multiple-parameter formulation in enhancing adaptivity and detail preservation under diverse blur conditions. Fig. 8 shows the deblurring results on the 4th frame of the 41th test sample from the GOPR0384\_11\_03 video sequence. The results indicate that the DMPJFRFTNet generates visually natural restorations with clear structural details and reduced artifacts.

Let  $\mathcal{I}_l$  and  $\mathcal{O}_l$  represent the input and output feature dimensions of the  $l$ -th layer, respectively.  $\mathcal{H}_l'$  and  $\mathcal{H}_l''$  stand for the hidden dimensions.  $h$  denotes the number of MLP units.  $K$  indicates the polynomial order for Chebyshev or Bernstein approximations.  $A_l$  is the count of attention heads, and  $E$  is the number of graph edges.  $S$  signifies the number of parallel stacks, while  $k$  denotes the propagation depth.  $l$  and  $s$  correspond to parameters for long and short scales,

TABLE V

SNR PERFORMANCE OF NEURAL NETWORK-BASED DENOISING METHODS  
(2D GFRFTNet, 2D GBFRFTNet, and JFRFTNet) UNDER VARIOUS  
GSOS FOR REAL-WORLD GRAPH SIGNALS.

	2D GFRFTNet	2D GBFRFTNet	JFRFTNet	DMPJFRFT-I-Net	DMPJFRFT-I-II-Net
<b>PEMSD7(M)</b>					
	$\sigma = 40$ (SNR=3.805)				
adj	16.090	16.102	17.345	<b>17.490</b>	16.695
lap	16.111	16.123	17.384	<b>17.466</b>	16.719
nor lap	16.073	16.086	17.303	<b>17.419</b>	16.643
row nor adj	16.065	16.077	17.289	<b>17.417</b>	16.676
sym nor adj	16.065	16.077	17.289	<b>17.417</b>	16.676
	$\sigma = 50$ (SNR=1.866)				
adj	15.813	15.826	16.882	<b>17.022</b>	16.421
lap	15.827	15.839	16.911	<b>17.002</b>	16.461
nor lap	15.799	15.813	16.835	<b>16.968</b>	16.401
row nor adj	15.795	15.808	16.829	<b>16.957</b>	16.408
sym nor adj	15.795	15.808	16.829	<b>16.957</b>	16.408
	$\sigma = 60$ (SNR=0.283)				
adj	15.568	15.561	16.578	<b>16.665</b>	16.18
lap	15.577	15.583	16.601	<b>16.679</b>	16.214
nor lap	15.558	15.552	16.531	<b>16.631</b>	16.159
row nor adj	15.555	15.546	16.529	<b>16.648</b>	16.173
sym nor adj	15.555	15.546	16.529	<b>16.648</b>	16.173
<b>PEMS08</b>					
	$\sigma = 200$ (SNR=1.741)				
adj	6.889	6.897	11.356	<b>12.382</b>	11.388
lap	9.317	9.32	12.308	13.95	<b>14.123</b>
nor lap	8.683	8.686	12.092	13.539	<b>13.929</b>
row nor adj	9.246	9.254	12.297	<b>13.451</b>	12.141
sym nor adj	8.694	8.697	12.098	<b>13.564</b>	12.433
	$\sigma = 240$ (SNR=0.157)				
adj	6.065	6.073	10.316	<b>11.790</b>	10.430
lap	8.848	8.851	11.51	<b>13.471</b>	12.155
nor lap	8.123	8.126	11.232	<b>12.972</b>	11.919
row nor adj	8.758	8.768	11.496	12.828	<b>12.927</b>
sym nor adj	8.135	8.137	11.243	<b>12.992</b>	12.620
	$\sigma = 280$ (SNR=−1.182)				
adj	5.412	5.419	9.466	<b>11.132</b>	9.049
lap	8.498	8.5	10.892	<b>13.098</b>	11.768
nor lap	7.701	7.704	10.556	<b>12.518</b>	11.301
row nor adj	8.389	8.399	10.872	<b>12.384</b>	12.313
sym nor adj	7.712	7.715	10.570	<b>12.339</b>	10.783
<b>Quality</b>					
	$\sigma = 50$ (SNR=3.148)				
adj	6.578	6.576	10.788	<b>10.859</b>	8.415
lap	6.862	6.867	11.228	<b>12.015</b>	11.189
nor lap	6.493	6.53	10.809	<b>11.977</b>	10.16
row nor adj	7.322	7.351	11.207	<b>11.881</b>	11.559
sym nor adj	6.020	6.082	10.495	<b>10.721</b>	10.618
	$\sigma = 80$ (SNR=−0.935)				
adj	4.323	4.320	8.154	<b>8.318</b>	7.525
lap	4.274	4.273	8.798	<b>9.746</b>	9.336
nor lap	4.129	4.168	8.265	<b>9.677</b>	8.678
row nor adj	4.869	4.901	8.803	<b>9.597</b>	9.127
sym nor adj	3.705	3.757	7.65	7.749	<b>8.302</b>
	$\sigma = 100$ (SNR=−2.873)				
adj	3.441	3.438	6.956	<b>7.078</b>	6.871
lap	3.246	3.244	7.59	<b>8.544</b>	8.393
nor lap	3.218	3.259	7.07	<b>8.553</b>	7.962
row nor adj	3.854	3.889	7.647	<b>8.439</b>	7.97
sym nor adj	2.841	2.887	6.378	6.386	<b>7.234</b>
<b>SST</b>					
	$\sigma = 15$ (SNR=2.956)				
adj	11.807	11.801	15.846	<b>19.005</b>	16.472
lap	15.015	15.019	19.145	<b>21.642</b>	16.912
nor lap	14.210	14.213	17.670	<b>21.650</b>	18.869
row nor adj	14.834	14.836	18.913	<b>21.543</b>	19.836
sym nor adj	14.237	14.235	17.688	<b>20.887</b>	18.891
	$\sigma = 20$ (SNR=0.457)				
adj	10.442	10.436	14.464	<b>17.192</b>	14.515
lap	13.543	13.544	17.778	<b>20.093</b>	15.972
nor lap	12.936	12.936	16.515	<b>19.905</b>	16.606
row nor adj	13.381	13.381	17.574	<b>19.822</b>	17.907
sym nor adj	12.959	12.957	16.543	<b>19.174</b>	16.631
	$\sigma = 25$ (SNR=−1.481)				
adj	9.385	9.378	13.423	<b>15.713</b>	12.995
lap	12.406	12.404	16.709	<b>18.772</b>	14.869
nor lap	11.926	11.923	15.625	<b>18.332</b>	14.437
row nor adj	12.257	12.255	16.523	<b>18.368</b>	16.110
sym nor adj	11.945	11.943	15.659	<b>17.628</b>	14.428

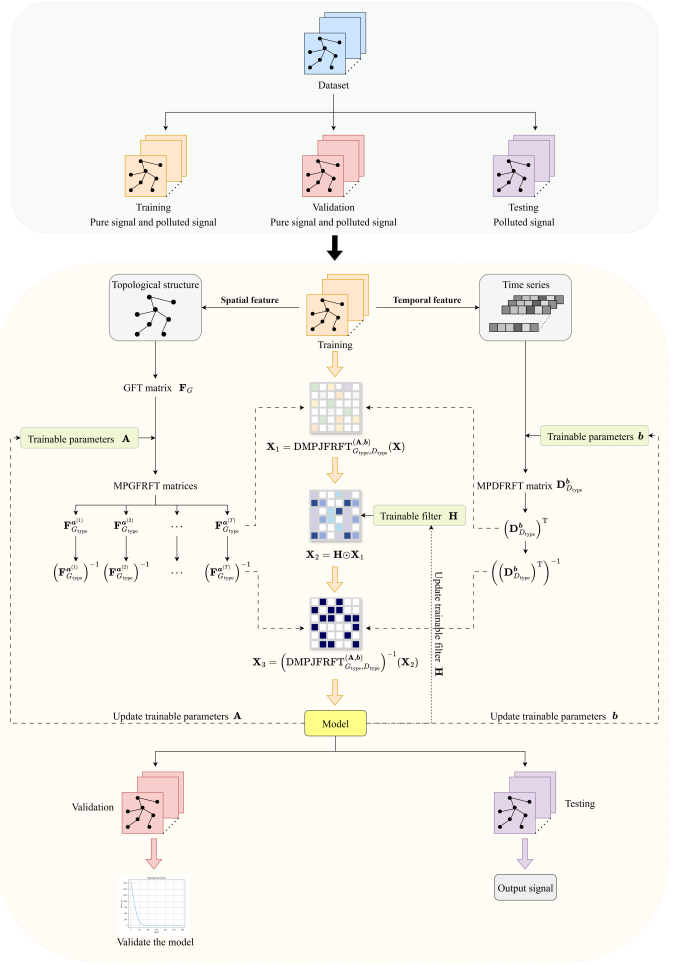


Fig. 6. Overall architecture of the proposed DMPJFRFTNet.

respectively.

For the  $l$ -th layer,  $\mathcal{I}_l$  and  $\mathcal{O}_l$  represent the input and output feature dimensions, respectively, while  $\mathcal{H}'_l$  and  $\mathcal{H}''_l$  correspond to the intermediate hidden dimensions. Let  $h$  denote the number of MLP units. The number of attention heads in this layer is denoted by  $A_l$ . The polynomial order used in Chebyshev or Bernstein approximations is indicated by  $K$ , and the total number of edges in the graph is represented by  $E$ .  $S$  denotes the number of parallel stacks employed in the architecture. Regarding propagation-related parameters,  $k$  specifies the propagation depth, whereas  $\ell$  and  $s$  correspond to the long-range and short-range propagation scales, respectively. Table IX presents the key characteristics of different implementations under both gradient descent-based filtering and neural network-based filtering.

## VI. CONCLUSION

In this paper, we introduced the DMPJFRFT, a novel framework for dynamic graph signal processing. Instead of using a single fractional order in each domain like JFRFT, the proposed DMPJFRFT leverages multiple-parameter mechanism to perform graph structure modeling in the spectral domain, thereby capturing the evolving topology and temporal dynamics of graph signals. To validate the effectiveness of

TABLE VI  
COMPARISON OF DENOISING PERFORMANCE BETWEEN THE PROPOSED DMPJFRFTNET MODELS (UNDER OPTIMAL GSOs) AND SEVERAL STATE-OF-THE-ART METHODS FOR GRAPH SIGNAL DENOISING.

	2D GFRFTNet	2D GBFRFTNet	JFRFTNet	APPNP	ARMAconv	BernNet	ChebyNet	GAT	GCN	LanczosNet	Specformer	SpectralCNN	UniMP	DMPJFRFT-I-INet	DMPJFRFT-I-IINet
PEMSD7(M)	$\sigma = 40$ 16.111	16.123	17.384	15.309	13.455	13.333	14.343	14.968	14.944	16.555	14.817	15.153	15.580	<b>17.490</b>	16.719
	$\sigma = 50$ 15.827	15.839	16.911	14.454	12.373	12.234	13.514	14.461	14.218	15.900	14.039	14.429	14.457	<b>17.022</b>	16.461
	$\sigma = 60$ 15.577	15.583	16.601	14.254	11.641	11.492	12.799	14.087	13.822	15.406	14.039	13.888	13.595	<b>16.679</b>	16.214
PEMS08	$\sigma = 200$ 9.317	9.320	12.308	10.701	10.35	10.682	10.553	10.331	10.28	12.945	10.094	12.434	10.739	13.95	<b>14.123</b>
	$\sigma = 240$ 8.848	8.851	11.51	9.609	9.623	9.595	9.425	9.364	9.306	12.565	9.000	11.886	9.653	<b>13.471</b>	12.927
	$\sigma = 280$ 8.498	8.500	10.892	8.763	8.772	8.753	8.553	8.578	8.524	12.209	8.311	11.426	8.783	<b>13.098</b>	12.313
Quality	$\sigma = 50$ 7.322	7.351	11.228	10.095	10.727	10.685	10.209	9.923	10.197	<b>12.337</b>	10.746	10.663	9.878	12.015	11.559
	$\sigma = 80$ 4.869	4.901	8.803	7.296	8.118	7.981	7.490	6.711	7.728	<b>10.197</b>	8.279	8.850	6.832	9.746	9.336
	$\sigma = 100$ 3.854	3.889	7.647	5.837	6.912	6.775	6.369	5.605	6.620	<b>9.162</b>	7.275	7.886	5.609	8.553	8.393
SST	$\sigma = 15$ 15.015	15.019	19.145	12.406	12.014	12.002	12.112	12.756	12.366	19.887	13.014	17.994	12.536	<b>21.650</b>	19.836
	$\sigma = 20$ 13.543	13.544	17.778	10.801	10.373	10.356	10.518	11.247	10.827	19.517	12.310	16.242	11.137	<b>20.093</b>	17.907
	$\sigma = 25$ 12.406	12.404	16.709	9.994	9.343	9.318	9.476	10.251	9.777	18.147	12.050	15.122	10.176	<b>18.772</b>	16.110

TABLE VII  
DENOISING PERFORMANCE OF NEURAL NETWORK-BASED METHODS ON FIVE REPRESENTATIVE VIDEOS FROM THE GOPRO DATASET.

	2D GFRFTNet	2D GBFRFTNet	JFRFTNet	APPNP	ARMAconv	BernNet	ChebyNet	GAT	GCN	LanczosNet	Specformer	SpectralCNN	UniMP	DMPJFRFT-I-INet	DMPJFRFT-I-IINet
GOPR0384_11_02	MSE 566.050	160.966	97.420	161.428	167.422	163.181	169.510	159.485	165.639	239.071	180.603	248.437	159.579	<b>90.392</b>	104.447
	PSNR 20.606	26.070	28.343	26.165	26.011	26.176	25.960	26.223	26.049	24.510	25.666	24.341	26.268	<b>28.670</b>	27.984
	SSIM 0.508	0.759	0.843	0.747	0.737	0.745	0.739	0.756	0.748	0.715	0.733	0.703	0.750	<b>0.858</b>	0.840
GOPR0384_11_03	MSE 583.758	144.908	84.206	147.814	153.157	148.478	153.906	143.720	147.345	184.127	163.275	170.041	144.334	<b>72.965</b>	81.592
	PSNR 20.477	26.532	28.070	26.485	26.329	26.515	26.309	26.688	26.521	25.616	26.050	25.986	26.662	<b>29.641</b>	29.114
	SSIM 0.366	0.636	0.636	0.752	0.620	0.609	0.618	0.612	0.636	0.625	0.638	0.602	0.667	0.629	<b>0.797</b>
GOPR0869_11_00	MSE 596.748	162.904	124.323	227.644	232.791	228.820	237.726	224.742	230.848	360.832	261.173	349.944	223.802	<b>113.112</b>	113.134
	PSNR 20.381	26.029	27.280	24.710	24.613	24.721	24.518	24.776	24.648	22.748	24.104	22.923	24.826	<b>27.736</b>	27.722
	SSIM 0.385	0.618	0.685	0.549	0.545	0.551	0.546	0.563	0.549	0.480	0.525	0.500	0.558	<b>0.719</b>	0.719
GOPR0396_11_00	MSE 586.621	214.140	142.820	188.790	195.849	194.451	200.790	190.093	201.145	387.963	221.714	431.951	186.439	<b>134.292</b>	164.029
	PSNR 20.454	24.831	26.754	25.516	25.368	25.433	25.246	25.479	25.243	22.612	24.839	22.118	25.605	<b>27.019</b>	26.054
	SSIM 0.508	0.698	0.790	0.720	0.715	0.719	0.714	0.726	0.715	0.626	0.703	0.605	0.724	<b>0.810</b>	0.768
GOPR0385_11_01	MSE 574.512	114.214	80.911	197.213	200.514	195.313	199.630	191.590	195.861	203.037	207.484	183.812	192.879	<b>70.785</b>	71.109
	PSNR 20.555	27.572	29.118	25.373	25.280	25.571	25.381	25.646	25.466	25.413	25.130	25.881	25.609	<b>29.744</b>	29.720
	SSIM 0.337	0.671	0.752	0.542	0.538	0.552	0.545	0.562	0.553	0.588	0.529	0.626	0.553	0.795	<b>0.796</b>

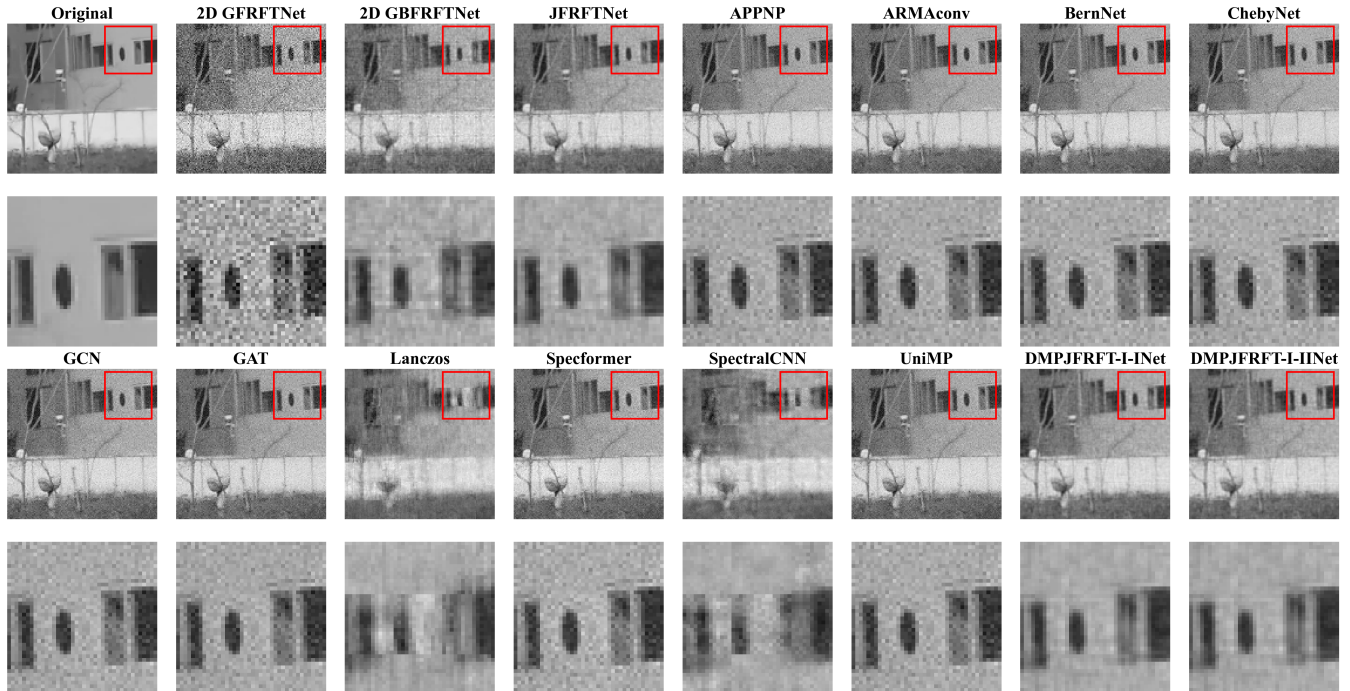


Fig. 7. Visual comparison of denoising results for Video GOPR0869\_11\_00.

TABLE VIII  
DEBLURING PERFORMANCE OF NEURAL NETWORK-BASED METHODS ON FIVE REPRESENTATIVE VIDEOS FROM THE GOPRO DATASET.

	2D GFRFTNet	2D GBFRFTNet	JFRFTNet	APPNP	ARMAconv	BernNet	ChebyNet	GAT	GCN	LanczosNet	Specformer	SpectralCNN	UniMP	DMPJFRFT-I-INet	DMPJFRFT-I-IINet	
GOPR0384_11_02	MSE	180.903	147.662	144.495	173.323	179.793	174.213	176.247	172.220	177.756	163.410	177.353	198.772	170.369	134.635	<b>133.289</b>
	PSNR	25.590	26.472	26.566	25.795	25.643	25.768	25.744	25.840	25.692	26.256	25.687	25.402	25.889	26.870	<b>26.914</b>
	SSIM	0.824	0.845	0.849	0.838	0.832	0.835	0.836	0.839	0.831	0.820	0.832	0.788	0.840	0.857	<b>0.858</b>
GOPR0384_11_03	MSE	87.148	74.411	72.512	82.200	84.203	84.529	84.181	82.024	86.288	105.673	85.821	124.151	81.820	67.279	<b>67.086</b>
	PSNR	28.839	29.505	29.610	29.075	28.973	28.966	28.976	29.088	28.883	28.100	28.879	27.459	29.113	29.951	<b>29.967</b>
	SSIM	0.870	0.869	0.874	0.879	0.879	0.877	0.876	0.882	0.867	0.806	0.869	0.789	0.881	0.885	<b>0.887</b>
GOPR0869_11_00	MSE	155.789	136.145	120.285	138.934	140.392	144.900	141.549	138.837	144.840	230.827	148.488	306.647	136.746	<b>117.242</b>	121.866
	PSNR	26.401	26.971	27.529	26.960	26.909	26.767	26.895	26.977	26.785	24.768	26.623	23.574	27.030	<b>27.643</b>	27.470
	SSIM	0.783	0.776	0.814	0.816	0.815	0.808	0.813	0.817	0.803	0.678	0.798	0.616	0.818	0.822	0.816
GOPR0396_11_00	MSE	286.229	244.930	236.859	265.566	274.670	272.340	267.527	258.628	273.445	307.239	276.074	427.161	259.784	223.677	<b>222.954</b>
	PSNR	23.584	24.264	24.401	23.909	23.759	23.798	23.878	24.024	23.799	23.645	23.735	22.160	24.009	24.659	<b>24.679</b>
	SSIM	0.759	0.773	0.782	0.787	0.779	0.779	0.783	0.792	0.776	0.728	0.775	0.651	0.791	0.797	<b>0.798</b>
GOPR0385_11_01	MSE	60.143	48.973	43.879	50.506	51.683	53.672	51.945	50.414	53.276	102.066	52.542	131.189	49.953	<b>41.451</b>	42.931
	PSNR	31.036	31.805	32.306	31.801	31.723	31.552	31.679	31.800	31.573	28.767	31.570	27.780	31.864	<b>32.555</b>	32.403
	SSIM	0.888	0.891	0.907	0.908	0.906	0.902	0.908	0.902	0.793	0.902	0.757	0.900	0.912	0.910	

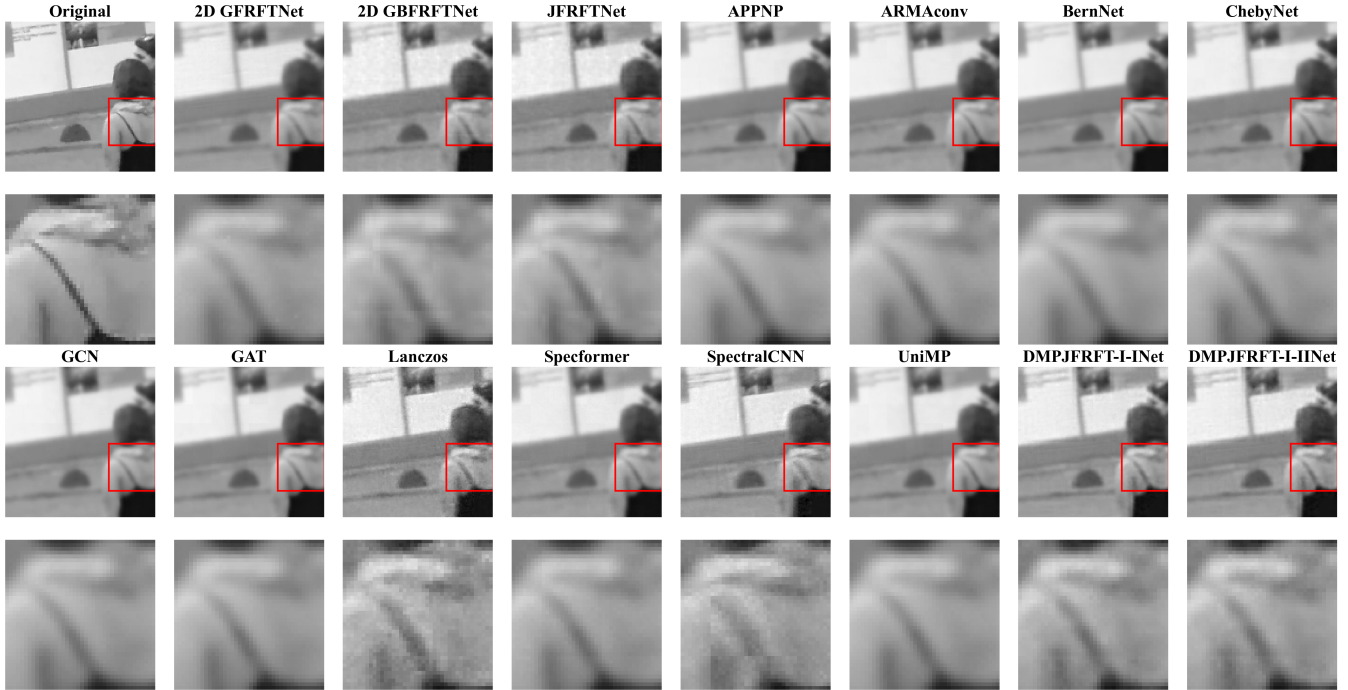


Fig. 8. Visual comparison of deblurring results for Video GOPR0384\_11\_03.

TABLE IX  
COMPARISON OF DIFFERENT FILTERING METHODS.

Method	Parameter Count	Feature Type	Complexity	Prior Information	Eigendecomposition	Dynamic
Gradient descent-based filtering						
2D GFRFT	$N + 1$	Spatio-spatial feature	$\mathcal{O}(N^3)$	Full	Yes	No
2D GBFRFT	$N + 2$	Spatio-spatial feature	$\mathcal{O}(N^3)$	Full	Yes	No
JFRFT	$N\mathcal{I} + 2$	Spatio-temporal feature	$\mathcal{O}(N^3)$	Full	Yes	No
DMPJFRFT	$2N\mathcal{I} + \mathcal{I}$	Spatio-temporal feature	$\mathcal{O}(N^3)$	Full	Yes	Yes
Neural network-based filtering						
2D GFRFTNet	$N + 1$	Spatio-spatial feature	$\mathcal{O}(N^3)$	Partial	Yes	No
2D GBFRFTNet	$N + 2$	Spatio-spatial feature	$\mathcal{O}(N^3)$	Partial	Yes	No
JFRFTNet	$N\mathcal{I} + 2$	Spatio-temporal feature	$\mathcal{O}(N^3)$	Partial	Yes	No
APPNP	$\mathcal{I}_t\mathcal{O}_t + \mathcal{O}_t$	Spatial feature	$\mathcal{O}(N\mathcal{I}\mathcal{O} + K\mathcal{E}\mathcal{I})$	Partial	No	No
ARMAconv	$S(2\mathcal{I}_t\mathcal{O}_t + (\mathcal{O}_t)^2 + \mathcal{O}_t)$	Spatial feature	$\mathcal{O}(Sk(2N\mathcal{I}\mathcal{O} + E\mathcal{I}))$	Partial	No	No
BernNet	$K + 1 + \mathcal{I}_t\mathcal{O}_t + \mathcal{O}_t$	Spatial feature	$\mathcal{O}(N\mathcal{I}\mathcal{O} + K\mathcal{E}\mathcal{I})$	Partial	No	No
ChebyNet	$(K + 1)\mathcal{I}_t\mathcal{O}_t + \mathcal{O}_t$	Spatial feature	$\mathcal{O}(N\mathcal{I}\mathcal{O} + K\mathcal{E}\mathcal{I})$	Partial	No	No
GAT	$A_t(\mathcal{I}_t\mathcal{O}_t + 2\mathcal{O}_t) + A_t\mathcal{O}_t$	Spatial feature	$\mathcal{O}(HN\mathcal{I}\mathcal{O} + H\mathcal{E}\mathcal{I})$	Partial	No	No
GCN	$\mathcal{I}_t\mathcal{O}_t + \mathcal{O}_t$	Spatial feature	$\mathcal{O}(N\mathcal{I}\mathcal{O} + E\mathcal{I})$	Partial	No	No
LanczosNet	$(2\ell + 2)h + \ell + \mathcal{O}_t + h^2 + (\ell + s)(\mathcal{O}_t)^2$	Spatial feature	$\mathcal{O}(N^3)$	Partial	Yes	No
Specformer	$3(\mathcal{O}_t)^2 + \mathcal{O}_t(\mathcal{I}_t + \mathcal{H}'_t + 2\mathcal{H}''_t + 5) + \mathcal{H}'_t + \mathcal{H}''_t$	Spatial feature	$\mathcal{O}(N^3)$	Partial	Yes	No
SpectralCNN	$\mathcal{I}_t\mathcal{O}_t + \mathcal{O}_t\mathcal{H}'_t N + \mathcal{H}'_t\mathcal{H}''_t$	Spatial feature	$\mathcal{O}(N^3)$	Partial	Yes	No
UniMP	$(4\mathcal{I}_t\mathcal{O}_t + \mathcal{O}_t)\mathcal{H}_t$	Spatial feature	$\mathcal{O}(N)$	Partial	No	No
DMPJFRFTNet	$2N\mathcal{I} + \mathcal{I}$	Spatio-temporal feature	$\mathcal{O}(N^3)$	Partial	Yes	Yes

**Algorithm 1** Training and Testing of DMPJFRFTNet

**Require:** Time-varying graph signal  $\mathbf{X} \in \mathbb{C}^{N \times TM}$ , noisy observation  $\mathbf{X}_{\text{noisy}}$ , learning rate  $\gamma$ , training epochs  $E$ , group size  $G$

**Ensure:** Learned transform parameters  $(\mathbf{A}^*, \mathbf{b}^*)$ , learned spectral filter  $\mathbf{H}^*$ , restored signal  $\tilde{\mathbf{X}}$ , evaluation metrics

- 1: Split dataset into training, validation, and test sets
- 2: Initialize fractional orders  $\mathbf{A} \leftarrow \mathbf{A}^{(0)}$ ,  $\mathbf{b} \leftarrow \mathbf{b}^{(0)}$  and filter  $\mathbf{H} \leftarrow \mathbf{H}^{(0)}$
- 3: **for** epoch = 1 to  $E$  **do**
- 4:   **Training Phase:**
- 5:     **for** each training batch **do**
- 6:       Forward pass:  
 $\mathbf{X}_{\text{batch}} \leftarrow \text{DMPJFRFTNet}(\mathbf{X}_{\text{noisy,batch}}, \mathbf{A}, \mathbf{b}, \mathbf{H})$
- 7:       Compute training loss:  
 $\mathcal{L}_{\text{train}} \leftarrow \|\tilde{\mathbf{X}}_{\text{batch}} - \mathbf{X}_{\text{batch}}\|_F^2 / NT$
- 8:       Backpropagation:  
 $\text{update } (\mathbf{A}, \mathbf{b}, \mathbf{H}) \text{ using Adam optimizer}$
- 9:     **end for**
- 10:   **Validation Phase:**
- 11:   Forward pass on validation set
- 12:   Compute validation metrics: (MSE, SNR) for real-data and (MSE, PSNR, SSIM) for videos
- 13: **end for**
- 14: **Testing:**
- 15: Load best parameters  $(\mathbf{A}^*, \mathbf{b}^*, \mathbf{H}^*)$
- 16: Forward pass on test set:  
 $\tilde{\mathbf{X}} \leftarrow \text{DMPJFRFTNet}(\mathbf{X}_{\text{noisy,test}}, \mathbf{A}^*, \mathbf{b}^*, \mathbf{H}^*)$
- 17: Compute evaluation metrics: (MSE, SNR) for real-data and (MSE, PSNR, SSIM) for videos

the proposed framework, we further developed two dynamic filtering strategies, namely a gradient descent-based filtering approach and a neural network implementation referred to as DMPJFRFTNet. Experimental evaluations on both real-world dynamic graph data and video datasets demonstrate that the DMPJFRFT achieves effective performance in denoising and deblurring tasks.

## REFERENCES

- [1] A. Ortega, *Introduction to Graph Signal Processing*. Cambridge University Press, 2022.
- [2] G. Leus, A. G. Marques, J. M. Moura, A. Ortega, and D. I. Shuman, "Graph signal processing: History, development, impact, and outlook," *IEEE Signal Process. Mag.*, vol. 40, no. 4, pp. 49–60, Jun. 2023.
- [3] A. Ortega, P. Frossard, J. Kovacevic, J. M. F. Moura, and P. Vандергейст, "Graph signal processing: Overview, challenges, and applications," *Proc. IEEE*, vol. 106, no. 5, pp. 808–828, Apr. 2018.
- [4] S. S. Saboktas, G. Mateos, and M. Cetin, "EEG-based emotion classification using graph signal processing," in *Proc. IEEE International Conference on Acoustics, Speech and Signal Processing (ICASSP)*, Jun. 2021, pp. 1065–1069.
- [5] G. Mateos, S. Segarra, A. G. Marques, and A. Ribeiro, "Connecting the dots: Identifying network structure via graph signal processing," *IEEE Signal Process. Mag.*, vol. 36, no. 3, pp. 16–43, May 2019.
- [6] S. Colonnese, M. Petti, L. Farina, G. Scarano, and F. Cuomo, "Protein-protein interaction prediction via graph signal processing," *IEEE Access*, vol. 9, pp. 142681–142692, Oct. 2021.
- [7] J. Ma, W. Huang, S. Segarra, and A. Ribeiro, "Diffusion filtering of graph signals and its use in recommendation systems," in *Proc. IEEE International Conference on Acoustics, Speech and Signal Processing (ICASSP)*, May 2016, pp. 4563–4567.
- [8] W. J. Xu, J. J. Liu, J. W. Yan, J. Yang, H. F. Liu, and T. Zhou, "Dynamic spatiotemporal graph wavelet network for traffic flow prediction," *IEEE Internet Things J.*, vol. 11, no. 5, pp. 8019–8029, Sep. 2024.
- [9] G. Qu, W. X. Hu, L. Xiao, J. Q. Wang, Y. T. Bai, B. Patel, K. Zhang, and Y. P. Wang, "Brain functional connectivity analysis via graphical deep learning," *IEEE Trans. Biomed. Eng.*, vol. 69, no. 5, pp. 1696–1706, Dec. 2022.
- [10] A. Sandryhaila and J. M. F. Moura, "Discrete signal processing on graphs," *IEEE Trans. Signal Process.*, vol. 61, no. 7, pp. 1644–1656, Jan. 2013.
- [11] A. Gavili and X. P. Zhang, "On the shift operator, graph frequency, and optimal filtering in graph signal processing," *IEEE Trans. Signal Process.*, vol. 65, no. 23, pp. 6303–6318, 2017.
- [12] K.-S. Lu and A. Ortega, "Fast graph Fourier transforms based on graph symmetry and bipartition," *IEEE Trans. Signal Process.*, vol. 67, no. 18, pp. 4855–4869, Aug. 2019.
- [13] J. Domingos and J. M. F. Moura, "Graph Fourier transform: A stable approximation," *IEEE Trans. Signal Process.*, vol. 68, pp. 4422–4437, Jul. 2020.
- [14] G. Patane, "Fourier-based and rational graph filters for spectral processing," *IEEE Trans. Pattern Anal. Mach. Intell.*, vol. 45, no. 6, pp. 7063–7074, May 2023.
- [15] W. F. Qi, S. R. Guo, and W. Hu, "Generic reversible visible watermarking via regularized graph Fourier transform coding," *IEEE Trans. Image Process.*, vol. 31, pp. 691–705, Dec. 2022.
- [16] Y. Q. Wang and B. Z. Li, "The fractional Fourier transform on graphs: Sampling and recovery," in *Proc. 14th IEEE International Conference on Signal Processing (ICSP)*, Aug. 2018, pp. 1103–1108.
- [17] C. Ozturk, H. M. Ozaktas, S. Gezici, and A. Koç, "Optimal fractional Fourier filtering for graph signals," *IEEE Trans. Signal Process.*, vol. 69, pp. 2902–2912, May 2021.
- [18] F. J. Yan and B. Z. Li, "Windowed fractional Fourier transform on graphs: Properties and fast algorithm," *Digit. Signal Process.*, vol. 118, p. 103210, Nov. 2021.
- [19] Y. C. Gan, J. Y. Chen, and B. Z. Li, "The windowed two-dimensional graph fractional Fourier transform," *Digit. Signal Process.*, vol. 162, p. 105191, Jul 2025.
- [20] T. Alikasifoglu, B. Kartal, and A. Koc, "Wiener filtering in joint time-vertex fractional Fourier domains," *IEEE Signal Process. Lett.*, vol. 31, pp. 1319–1323, May 2024.
- [21] T. Alikasifoglu, B. Kartal, E. Ozgunay, and A. Koc, "Joint time-vertex fractional Fourier transform," *Signal Process.*, vol. 233, p. 109944, Aug. 2025.
- [22] F. Grassi, A. Loukas, N. Perraudin, and B. Ricaud, "A time-vertex signal processing framework: Scalable processing and meaningful representations for time-series on graphs," *IEEE Trans. Signal Process.*, vol. 66, no. 3, pp. 817–829, Nov. 2018.
- [23] A. Loukas and D. Foucard, "Frequency analysis of time-varying graph signals," in *Proc. IEEE Global Conference on Signal and Information Processing (GlobalSIP)*, Dec. 2016, pp. 346–350.
- [24] Z. Q. Yan and Z. C. Zhang, "Trainable joint time-vertex fractional Fourier transform," *arXiv preprint arXiv:2507.21527*, 2025.
- [25] M. J. Cui, Z. C. Zhang, and W. Yao, "Multiple-parameter graph fractional Fourier transform: Theory and applications," *arXiv preprint arXiv:2507.23570*, 2025.
- [26] X. J. Kang, R. Tao, and F. Zhang, "Multiple-parameter discrete fractional transform and its applications," *IEEE Transactions on Signal Processing*, vol. 64, no. 13, pp. 3402–3417, Mar. 2016.
- [27] F. M. Bianchi, D. Grattarola, L. Livi, and C. Alippi, "Graph neural networks with convolutional arma filters," *IEEE Trans. Pattern Anal. Mach. Intell.*, vol. 44, no. 7, pp. 3496–3507, Jan. 2022.
- [28] J. Y. Chen, Y. Zhang, and B. Z. Li, "Graph linear canonical transform: Definition, vertex-frequency analysis and filter design," *IEEE Trans. Signal Process.*, vol. 72, pp. 5691–5707, Dec. 2024.
- [29] E. Isufi, F. Gama, D. I. Shuman, and S. Segarra, "Graph filters for signal processing and machine learning on graphs," *IEEE Transactions on Signal Processing*, vol. 72, pp. 4745–4781, Jan. 2024.
- [30] S. N. Guo, Y. F. Lin, H. Y. Wan, X. C. Li, and G. Cong, "Learning dynamics and heterogeneity of spatial-temporal graph data for traffic forecasting," *IEEE Trans. Knowl. Data Eng.*, vol. 34, no. 11, pp. 5415–5428, Feb. 2022.
- [31] Z. Q. Yan and Z. C. Zhang, "Jfrffnet: A data-model co-driven graph signal denoising model with partial prior information," *arXiv preprint arXiv:2509.09147*, 2025.
- [32] K. Yi, Q. Zhang, W. Fan, S. J. Wang, P. Y. Wang, H. He, N. An, D. F. Lian, L. B. Cao, and Z. D. Niu, "Frequency-domain MLPs are more effective learners in time series forecasting," in *Proc. Advances in*

*Neural Information Processing Systems (NeurIPS)*, vol. 36, Dec. 2023, pp. 76 656–76 679.

[33] J. Giraldo, A. Mahmood, B. Garcia-Garcia, D. Thanou, and T. Bouwmans, “Reconstruction of time-varying graph signals via Sobolev smoothness,” *IEEE Trans. Signal Inf. Process. Netw.*, vol. 8, pp. 201–214, Mar. 2022.

[34] F. J. Yan and B. Z. Li, “Multi-dimensional graph fractional Fourier transform and its application to data compression,” *Digit. Signal Process.*, vol. 129, p. 103683, Sep. 2022.

[35] S. Son, S. Lee, S. Nah, R. Timofte, and K. M. Lee, “Ntire 2021 challenge on video super-resolution,” in *Proc. Computer Vision and Pattern Recognition (CVPR)*, Jun. 2021, pp. 166–181.

[36] J. Gasteiger, A. Bojchevski, and S. Günnemann, “Gasteiger, johannes and bojchevski, aleksandar and gunnemann, stephan,” in *Proc. International Conference on Learning Representations (ICLR)*, May 2019.

[37] M. G. He, Z. W. Wei, and H. T. Xu, “Bernnet: Learning arbitrary graph spectral filters via bernstein approximation,” in *Proc. Advances in neural information processing systems (NeurIPs)*, vol. 34, Dec. 2021, pp. 14 239–14 251.

[38] P. Velickovic, G. Cucurull, A. Casanova, A. Romero, P. Lio, and Y. Bengio, “Graph attention networks,” *arXiv preprint arXiv:1710.10903*, 2017.

[39] B. Jiang, Z. Y. Zhang, D. D. Lin, J. Tang, and B. Luo, “Semi-supervised learning with graph learning-convolutional networks,” in *Proc. Computer Vision and Pattern Recognition (CVPR)*, 2019, pp. 11 313–11 320.

[40] R. J. Liao, Z. Z. Zhao, R. Urtasun, and R. S. Zemel, “LanczosNet: Multi-scale deep graph convolutional networks,” in *Proc. International Conference on Learning Representations (ICLR)*, Dec. 2019.

[41] D. Y. Bo, C. Shi, L. L. Wang, and R. J. Liao, “Specformer: Spectral graph neural networks meet transformers,” in *Proc. International Conference on Learning Representations (ICLR)*, Feb. 2023.

[42] X. Y. Wang and M. H. Zhang, “How powerful are spectral graph neural networks,” in *Proc. International conference on machine learning (ICML)*, vol. 162, Jul. 2022, pp. 23 341–23 362.

[43] H. R. Wang, H. T. Yin, M. H. Zhang, and P. Li, “Equivariant and stable positional encoding for more powerful graph neural networks,” in *Proc. International Conference on Learning Representations (ICLR)*, Apr. 2022.

[44] Y. S. Shi, Z. J. Huang, S. K. Feng, H. Zhong, W. J. Wang, and Y. Sun, “Masked label prediction: Unified message passing model for semi-supervised classification,” in *Proc. International Conference on Learning Representations (ICLR)*, May 2021.

[45] S. Nah, T. Hyun Kim, and K. Mu Lee, “Deep multi-scale convolutional neural network for dynamic scene deblurring,” in *Proc. Computer Vision and Pattern Recognition (CVPR)*, Jul. 2017, pp. 3883–3891.

**Zhichao Zhang** (Member, IEEE) received the B.S. degree in mathematics and applied mathematics from Gannan Normal University, Ganzhou, Jiangxi, China, in 2012, and the Ph.D. degree in mathematics of uncertainty processing from Sichuan University, Chengdu, Sichuan, China, in 2018. From September 2017 to September 2018, he was a Visiting Student Researcher with the Department of Electrical and Computer Engineering, Tandon School of Engineering, New York University, Brooklyn, NY, USA, where he was awarded a grant from the China Scholarship Council. Since 2019, he has been with the School of Mathematics and Statistics, Nanjing University of Information Science and Technology, Nanjing, Jiangsu, China, where he is currently a Full Professor and a Ph.D Supervisor. From January 2021 to January 2023, he was a Macau Young Scholars Post-Doctoral Fellow of information and communication engineering with the School of Computer Science and Engineering, Macau University of Science and Technology, Macau, SAR, China. He has published more than 60 journal articles in IEEE TRANSACTIONS ON INFORMATION THEORY, IEEE TRANSACTIONS ON SIGNAL PROCESSING, IEEE SIGNAL PROCESSING LETTERS, IEEE COMMUNICATIONS LETTERS, Signal Processing, and Journal of Fourier Analysis and Applications. His current research interests include mathematical theories, methods, and applications in signal and information processing, including fundamental theories, such as Fourier analysis, functional analysis and harmonic analysis, applied theories, such as signal representation, sampling, reconstruction, filter, separation, detection and estimation, and engineering technologies, such as satellite communications, radar detection, and electronic countermeasures. He was a member of the International Association of Engineers, the China Society for Industrial and Applied Mathematics, the Chinese Institute of Electronics, and the Beijing Society for Interdisciplinary Science. He was the Vice President of the Jiangsu Society for Computational Mathematics and the Director of the Jiangsu Society for Industrial and Applied Mathematics. He was listed among world’s top 2% scientists recognized by Stanford University in 2021 and 2022.

**Manjun Cui** received the B.S. degree in Mathematics and Applied Mathematics from Yancheng Teachers University, Yancheng, Jiangsu, China, in 2022. She is currently pursuing the Ph.D. degree in mathematics with the School of Mathematics and Statistics, Nanjing University of Information Science and Technology, Nanjing, Jiangsu, China.

**Ziqi Yan** received the B.S. degree in Mathematics and Applied Mathematics from Yancheng Teachers University, Yancheng, Jiangsu, China, in 2023. He is currently pursuing the M.S. degree in mathematics with the School of Mathematics and Statistics, Nanjing University of Information Science and Technology, Nanjing, Jiangsu, China.

**Yangfan He** received the Ph.D. degree in space physics from Wuhan University, Wuhan, China, in 2022. She is currently a Lecturer with the School of Information and Communication Engineering, Nanjing Institute of Technology, Nanjing, Jiangsu, China. Her current research interests include signal processing, plasma waves, and magnetosphere-ionosphere coupling.